When Trade Burns the Air: The Welfare Consequences of Agricultural Trade Liberalization[†]

Fangyuan Peng, Guojun He, Yuhang Pan

Jan 2026

[Latest version]

Abstract

Trade liberalization generates economic gains, but production can impose environmental costs both domestically and across borders—raising the question of whether pollution costs discount trade benefits and how costs are distributed internationally. This paper develops a framework to quantify these trade-offs in Southeast Asian agricultural exports, where fire-based land clearing has intensified with trade expansion. We show that export growth significantly increases fire activity, particularly on high-potential agricultural land. Using atmospheric transport modeling to simulate dispersion from millions of fires over the last two decades, we find that fire-induced pollution exposes populations within Southeast Asian countries and across more than 40 downwind countries. Embedding these costs into a general equilibrium model enables welfare comparison. We find that each dollar of export growth generates $0.11 in global pollution damages, with health costs offsetting a substantial share of trade gains—demonstrating that the domestic and international distribution of environmental externalities is essential to evaluate trade welfare.

Keywords: Agricultural Trade, Environmental Externalities, Transboundary Pollution

JEL Codes: F18, F64, Q17, Q56

[†]He: Faculty of Business and Economics, University of Hong Kong (email: gjhe@hku.hk); Pan: Peking University (email: yhpan@pku.edu.cn); Peng: Faculty of Business and Economics, University of Hong Kong (email: pengfy@hku.hk). We would like to thank Yatang Lin, Jin Wang and seminar participants at the University of Hong Kong, Shanghai Jiaotong University, and Nanjing University. Financial support from the Research Grants Council of Hong Kong through the Theme-based Research Scheme (T24-508/22-N) and the Junior Research Fellow Scheme is gratefully acknowledged. All errors are our own.

1 Introduction

Over the past few decades, trade liberalization has driven the production of agricultural products and resource-intensive activities to relocate from high-income to developing economies (e.g., Hanson 2012; Dicken 2015).[1] While this reallocation expanded global gains from trade, it has also heightened environmental damages, including elevated greenhouse gas (GHG) emissions and pollution that is both locally concentrated and transboundary in its impacts (e.g., Shapiro 2016). This tension has motivated the widely discussed "pollution haven" and a wave of "green trade" policies, such as carbon border adjustments and sustainable supply-chain standards, which are designed to internalize environmental damages that cross national boundaries.[2] Yet a central challenge remains unresolved: How do we quantify the environmental externalities embedded in international trade, and how large are these costs relative to the gains from trade, particularly when trade-induced pollution generated in one country is physically transported to another?

The agricultural fires in Southeast Asia (SEA) provide an ideal setting for examining the environmental externalities in international trade. The region has experienced rapid export-driven agricultural expansion since 1995, with trade volumes increasing sixfold while production tripled and the cultivated area grew by 50%. Despite this growth, much of the expansion still relies on fire-based land clearing, operating under weak environmental regulations (e.g., Dipoppa and Gulzar 2024). Consequently, the region has become a global hotspot for agricultural fires. For example, during March 2023, a peak month in the land-clearing

[1] For example, the share of global agricultural output produced in high-income countries decreased from 73.13% to 59.89% between 1995 and 2020 (Figure A1); similarly, manufacturing capacity shifted substantially toward Asia.

[2] Academic research distinguishes between the pollution haven effect (PHE) and the pollution haven hypothesis (PHH). The PHE posits that differences in environmental regulation create comparative advantage and thus influence production and trade patterns, whereas the PHH links these regulatory differences to trade liberalization, predicting that lower trade costs will lead pollution-intensive activities to concentrate in countries with weaker regulations. While the PHE has received empirical support, evidence on the PHH remains mixed. See, for example, Copeland (2008); Duan et al. (2021); Cherniwchan, Copeland and Taylor (2017); Copeland and Taylor (2004, 2003).

season, Southeast Asia accounted for 27% of worldwide fire activity despite occupying only 3% of global land area. Moreover, cross-border pollution from these fires has been extensively documented[3], affecting over 4 billion people in downwind countries across Asia, representing more than half the world's population (Figure A2). The confluence of rapid trade liberalization, reliance on fire-based land clearing, and extensive transboundary pollution dispersion makes this setting uniquely suited for quantifying the distribution of environmental costs across pollution-generating and pollution-receiving countries.

Quantifying these externalities requires comparing environmental costs against trade benefits within a unified welfare framework. We develop such a framework by jointly accounting for the gains from trade and the environmental damages from fire-related pollution. Building on Shapiro (2016), we model environmental damages as entering a discounted utility function, allowing pollution exposure in both producing and downwind countries to affect welfare. We then embed this environmental damage term within a trade-based welfare expression derived from the ACR framework (Arkolakis, Costinot and Rodríguez-Clare 2012), so that welfare can be expressed in terms of observable trade shares, trade elasticities, and measured cross-border pollution spillovers. This welfare framework allows us to identify gains from trade and losses from pollution, quantify their distribution across countries, and simulate welfare changes under alternative policy scenarios.

To obtain the parameters that characterize environmental damage in our welfare framework, we construct a grid-level empirical pipeline linking export expansion to health costs via fire activity and transboundary pollution dispersion. We first exploit spatial variation in land suitability—measured using the FAO's Global Agro-Ecological Zones dataset—to identify the causal effect of export growth on fires. Our identification strategy compares how areas with different comparative advantages respond to trade shocks within each country. We then employ the HYSPLIT atmospheric transport model to trace emissions from fires

[3]See, e.g., Reuters (2023); Azmi (2025); Jong (2025); Sheldon and Sankaran (2017). More details are discussed in Section 2.

to affected populations, generating over 300 million seven-day trajectories under observed wind fields. This source-receptor mapping allows us to translate fire increases into incremental $PM_{2.5}$ concentrations at each location and subsequently into monetized health damages, capturing both domestic and transboundary pollution impacts. Combining our estimates of trade-induced fire responses with this dispersion modeling yields the marginal environmental damage per dollar of agricultural export expansion.

Exploiting within-country spatial variation in land suitability, we causally identify the effect of export expansion on land-clearing fires. Comparing lands with different suitability levels within the same country and year, we find that a 1% increase in agricultural exports leads to a 6.5% increase in fire activity on highly suitable land relative to less suitable land, consistent with export-driven agricultural intensification concentrating on lands with comparative advantage. Moreover, to link this response to trade policy, we use the simple average Most Favored Nation (MFN) tariff rate across all importers of Southeast Asian countries as a proxy for trade liberalization. We find that a one-percentage-point reduction in tariffs leads to a 0.18%–0.37% increase in fire activity on high-suitability land relative to low-suitability land. We then trace the pollution footprint of these export-induced fires. Simulating atmospheric dispersion from all grid cells across Southeast Asia using HYSPLIT modeling, we find that pollution from the region can reach over 40 downwind countries, potentially affecting more than 4 billion people.[4] Combining these dispersion patterns with nearly 4 million detected fires over 2003–2021 and over 40 billion $PM_{2.5}$ observations, we show that emissions from agricultural fires routinely travel for up to seven days across borders, generating substantial domestic and transboundary increases in $PM_{2.5}$ concentrations. Combining atmospheric dispersion patterns with our fire response estimates, we construct a source-receptor matrix mapping trade-induced fires from each grid to downwind health damages. We find that marginal pollution costs account for over 10% of export value. Ag-

[4]Figure A2 illustrates the population distribution in regions potentially exposed to pollution from Southeast Asia. In total, these affected areas impact approximately 4.2 billion people globally.

gregating to country pairs reveals widespread but highly uneven pollution spillovers: while emissions reach over 40 countries, neighboring countries bear disproportionate costs. Southeast Asian countries themselves absorb 80% of total health damages from within-region fires, while China, India, Bangladesh, and Japan account for the majority of the remaining 20% of extra-regional costs.

Lastly, we incorporate these damages into our welfare framework, which places the gains from trade and the environmental costs of fire-induced pollution on a common metric. Relative to a counterfactual without trade-driven production reallocation, on average, pollution costs represent 2.32% of trade gains, rising to 13.45% among pollution-receiving countries and ranging from 0% to more than 200% across individual countries. This distribution is highly uneven: downwind populated countries such as China and India bear substantial pollution damages that in some cases exceed trade benefits, while long-distance countries such as the USA benefit from trade with SEA countries without pollution exposure.

This paper provides a textbook example of an environmental externality arising from international trade. Export expansion triggers agricultural fires that release emissions traveling across borders, exposing downwind populations to air pollution regardless of whether they participate in or benefit from the underlying trade. This exemplifies a fundamental departure from standard bilateral trade analysis: the welfare consequences extend to all countries physically exposed to pollution, not just trading partners. We develop an integrated framework combining atmospheric dispersion modeling with quantitative trade theory to trace and quantify these multilateral externalities, showing that even one production margin—agricultural fires—generates pollution damages that substantially erode the benefits of trade liberalization.

Our results underscore the importance of multilateral environmental policies that account for trade's cross-border externalities rather than restricting trade itself. Identifying the spatial distribution of damages and their sources provides the foundation for policies such as carbon border adjustments, transboundary pollution compensation schemes, and regional

environmental agreements (e.g., Dasgupta and Ehrlich 2013; Fontagné and Schubert 2023; Clausing and Wolfram 2023; Wang, Xu and Chen 2025). By quantifying both the origin and incidence of pollution, our framework offers a basis for more equitable and efficient coordination between trade and environmental policy. Further tariff reductions or trade expansion would exacerbate pollution damages in countries only marginally involved in agricultural trade, who bear environmental costs without sharing economic benefits yet have limited bargaining power in negotiations. Quantifying these distributional consequences provides the empirical foundation for policies that internalize externalities—such as linking market access to emission standards or establishing regional compensation mechanisms funded by export revenues.

We make several contributions to the literature. First, this paper develops a new empirical framework to evaluate environmental externalities in trade, which extends the analysis from bilateral trading pairs to the full set of pollution-receiving countries. A clear and comprehensive measure of externality has been difficult because it requires the creation of a joint link between the origins of production and pollution, the nature of pollutant transmission, and the identification of all parties who are ultimately exposed. As a result, existing empirical research has typically examined one part of this chain at a time. Some studies, for example, quantify emissions or land-use externalities within the exporter's national borders (Bombardini and Li 2020; Tanaka, Teshima and Verhoogen 2022; Carreira, Costa and Pessoa 2024; Du, Li and Zou 2024; Rodrigue, Sheng and Tan 2024). Some other works examine environmental impacts in the importing country, particularly focusing on how import competition or import substitution affects domestic pollution levels (Gutiérrez and Teshima 2018; Shi and Zhang 2023; Akerman, Forslid and Prane 2024). Only a few studies explicitly incorporate pollution into quantitative trade frameworks globally, focusing primarily on CO_2 emissions from international transport (Cristea et al. 2013; Shapiro 2016; Larch and Wanner 2017). In this study, we introduce a general framework in which trade reallocates externalities with heterogeneity in space. We show that, using a state-of-the-art atmospheric

transport model, one can construct a source–receptor matrix mapping externality in each origin country to exposure in each downwind region, making the externality spatially explicit and empirically traceable.

Secondly, this paper extends the pollution haven literature beyond manufacturing to the agricultural sector. While prior research has focused on how trade liberalization relocates industrial pollution through cross-border shifts in manufacturing production (e.g., Ederington, Levinson and Minier 2005; Kellenberg 2009, 2012; Fowlie, Reguant and Ryan 2016; Cherniwchan, Copeland and Taylor 2017), we provide the first systematic evidence of analogous dynamics in agriculture. Specifically, we show that export growth in Southeast Asia intensifies agricultural burning as a marginal technology of expansion, creating pollution havens through land-based production rather than factory relocation. This finding highlights how trade-induced agricultural expansion generates environmental externalities through previously unexplored channels.

Furthermore, we contribute to the measurement of transboundary pollution impacts and the identification of environmental externality spillovers. Existing studies typically infer cross-border pollution indirectly—using wind interactions, episodic events, or spatial correlations—to capture atmospheric transport patterns (e.g., Cheung, He and Pan 2020; Jia and Ku 2019; Sheldon and Sankaran 2017). Recent studies employ more sophisticated modeling, specifically the HYSPLIT atmospheric transport model, to fully trace pollution dispersion, but limit their analysis to tracing pollution sources for individual receptor countries (e.g., Heo, Ito and Kotamarthi 2025; Lee, Wilson and Hsiang 2025). We advance this literature by developing a grid-to-grid multiple source-receptor framework based on the HYSPLIT model, which maps pollution flows from all agricultural fires in Southeast Asia to all downwind receptors at high resolution. By linking pollution trajectories with $PM_{2.5}$ concentrations and health outcomes, we quantify the magnitude and reach of transboundary pollution spillovers, providing key parameters for welfare analysis.

The remainder of the paper is organized as follows. Section 2 provides background on

agricultural trade and burning practices in Southeast Asia. Section 3 presents the theoretical framework. Section 4 describes the data sources and key variables. Section 5 reports the empirical estimates of how agricultural exports affect fire activity. Section 6 quantifies the transmission of fire emissions and their effects on both local and downwind air quality. Section 7 applies the model to evaluate the welfare gains from trade and the associated environmental externalities. Section 8 concludes.

2 Background

2.1 Agricultural Trade and Cropland Expansion in Southeast Asia

Since the establishment of the World Trade Organization (WTO) in 1995, global agricultural trade has experienced rapid growth, with countries in Southeast Asia witnessing some of the most significant transformations. This rapid increase in agricultural trade can be largely attributed to trade liberalization and the reduction of trade barriers. As shown in Figure A3, average agricultural tariffs were reduced by 25%, significantly improving market access for agricultural exports in Southeast Asia. Consequently, agricultural exports in the region have increased more than sixfold since 1995.

The surge in agricultural trade in Southeast Asia has been largely driven by the region's comparative advantage in agro-food production, especially given its tropical climate, which is well-suited to cultivating a range of crops such as rice, oil palm, fruits, and rubber. Southeast Asia's natural endowments, combined with relatively low labor costs, have enabled countries in the region to rapidly expand their agricultural sectors. Rice cultivation remains the backbone of agricultural production in the region, accounting for a significant share of the total agricultural output. Moreover, other crops, particularly oil palm, have grown increasingly important, with the region becoming a global leader in palm oil production. As a result, Southeast Asian countries have capitalized on their comparative advantage by increasing exports of key agricultural products, including rice, palm oil, rubber, and tropical

fruits.

This expansion in agricultural trade has been a key factor driving the growth of agricultural production in Southeast Asia. According to Figure A4 Panel A, agricultural production in the region, measured in tons, has more than tripled since 1995. Laos experienced the highest growth in production, increasing by more than 7 times, followed by Cambodia, which grew by 6 times. Growth in production drives the increase in agricultural land use. Between 1995 and 2021 (Figure A4 Panel B), agricultural land across Southeast Asia expanded by more than 50%. Laos and Cambodia saw the largest increases, with agricultural land growing by 126% and 123%, respectively. Indonesia, Malaysia, and Myanmar saw substantial growth in agricultural land, with increases of around 50%, while Indonesia and Myanmar experienced the largest expansion in absolute terms. However, this expansion often came at the expense of forests. Much of the agricultural land expansion in Southeast Asia has been driven by the conversion of forests and other natural lands into agricultural areas or plantation crops. Additionally, fire has been a common method used in land transformation, further exacerbating environmental challenges.

2.2 Fire as a Common Agricultural Practice in Southeast Asia

In Southeast Asia, fires are used as a common tool for agricultural management. Farmers use fire to clear agricultural residues, such as crop stubble left after rice and sugarcane harvesting, and to remove weeds that compete with crops. Fire is also frequently used to cut and burn vegetation in preparation for land cultivation, a practice commonly known as "slash-and-burn" (BBC 2013).

Burning is widely regarded as a cost-effective method for land clearing in developing countries, particularly in Southeast Asia, where it is commonly used by farmers. The process is relatively inexpensive, costing approximately $5 per hectare. It requires minimal time and effort, and can be carried out by unskilled labor, making it highly accessible for smallholder farmers with limited resources. Fire can also help eliminate pests and weeds, including

insects, larvae, and pathogens that may otherwise harm crops. Moreover, fire helps replenish soil nutrients, as the ash from burned vegetation serves as a natural fertilizer, enriching the soil with essential minerals such as potassium and phosphorus. In contrast, mechanical clearing is far more costly and resource-intensive. This method can cost as much as $250 per hectare—50 times more expensive than burning (Devex 2019). It requires significant time to clear the land and handle post-clearance activities, such as leveling the ground and preparing the soil for planting. Additionally, it necessitates skilled labor to operate complex machinery, such as bulldozers or tractors, and requires ongoing maintenance and fuel, further increasing the costs. The high cost and reliance on specialized operators make mechanical clearing a less viable option for small-scale farmers with limited resources. Therefore, the agricultural fires is an attractive option in areas where financial constraints, limited access to technology, and labor availability are significant factors. Even larger agricultural companies, which may have access to more resources, still prioritize cost-effectiveness in their operations. Since mechanical clearing is far more expensive, many large-scale farms in regions with weak environmental regulations may opt for burning as the quicker and cheaper method for land preparation.

Southeast Asia is a global hotspot for agricultural fires, characterized by distinct seasonal patterns. As illustrated in Figure A5, fire activity in this region is highly seasonal, peaking during the dry, pre-monsoon months from January to May. This seasonal pattern is most pronounced in mainland Southeast Asia, including Cambodia, Laos, Myanmar, and Thailand, where a single intense burning season typically occurs between February and April. This period coincides with the end of the dry season, making it an ideal time for farmers to clear crop residues and prepare land for the upcoming wet-season planting. In contrast, maritime Southeast Asia, including Indonesia and Malaysia, experiences a bimodal fire pattern. These regions see two major peaks in fire activity: one during the primary dry season from August to October and another smaller peak in February and March. This dual peak is due to the region's equatorial climate, which has two distinct dry periods. With multiple crop-

ping cycles per year and short turnaround times, farmers often rely on fire as the quickest method to clear land between planting seasons. In Southeast Asia, fire is commonly used for land clearing and pest control across a wide range of crops. In Indonesia and Malaysia, the expansion of oil palm plantations has been a major driver of land conversion, with fires often used to clear forests for new plantations. Similarly, rice and sugarcane, both of which are land-intensive crops, contribute significantly to fire activity in this region. This is primarily because farmers burn waste or straw left behind after harvest, a practice that is both efficient and cost-effective in preparing the land for subsequent planting.

However, agricultural burning is a significant source of pollution. As shown in Figure A6, agricultural waste burning is a major contributor to global $PM_{2.5}$ emissions. Exposure to smoke from fires is associated with adverse health outcomes, including morbidity and mortality (Rangel and Vogl 2019; He, Liu and Zhou 2020; Zivin et al. 2020; Garg, Jagnani and Pullabhotla 2024; Borgschulte, Molitor and Zou 2024). Also, recent research has shown that agricultural waste burning produces more harmful particulate matter than other combustion sources, highlighting that the health impacts per unit of exposure may exceed those from other sources (Zheng et al. 2025).

In addition, fire-induced pollution affects not only the health of local populations but also the health of people in neighboring downwind countries. The transboundary haze pollution has been a long-standing issue in Southeast Asia, affecting air quality both within the countries where the fires occur and in neighboring regions.[5] During the burning season, fires in Mainland Southeast Asia, which contribute up to 80% of aerosols and 49% of PM10 concentrations, are transported long-range to China (Zhu et al. 2016; Vongruang and Pimonsree 2020). Although SEA countries and the Association of Southeast Asian Nations (ASEAN) have signed various agreements to address the issue, the region has yet to effectively resolve the problem, and haze pollution remains a persistent challenge (Reuters 2023; Azmi 2025;

[5]Sheldon and Sankaran (2017) shows that Indonesian forest burning increases polyclinic visits for respiratory and cardiovascular illnesses in Singapore, highlighting transboundary pollution's health impacts.

Jong 2025).[6].

The increasing agricultural trade might worsen the situation. As shown in Figure A7, since the establishment of the WTO in 1995, burning areas in the SEA region have increased by about 60%, with a particularly significant rise after the 2000s. This sharp turn parallels the pattern observed in Figure A3, where agricultural exports show a negligible increase before 2000, followed by a sharp rise after 2000. Moreover, Figure A8 illustrates the positive relationship between the log of agricultural exports and the log of fire occurrences at the country-year level. This suggests that trade liberalization, which boosted agricultural exports after 2000, may have contributed to the surge in fires by encouraging the expansion of agricultural areas through burning. This kind of fire activity could potentially offset the benefits brought about by trade. In the following sections, we will first model how these environmental externalities influence utility and welfare. Then, we will incorporate real-world data into the model, starting by verifying how trade impacts fire activities in different regions. Next, we will calculate the externalities resulting from these fire activities, and finally, assess how these externalities affect welfare in the model.

3 Model of Trade and Environment

Our objective is to quantify how international trade in agricultural goods affects welfare when production in one country generates airborne pollution that affects populations in other countries. Evaluating these effects requires a framework that links two channels: (i) how trade policy reshapes the global allocation of agricultural production, and (ii) how the

[6]ASEAN signed the Agreement on Transboundary Haze Pollution in 2002 (ASEAN 2002). In 2016, ASEAN established the 'Roadmap on ASEAN Cooperation towards Transboundary Haze Pollution Control with Means of Implementation', which was implemented until 2023 (ASEAN 2024*b*). A second roadmap, covering the period from 2023 to 2030, aims to strengthen regional measures to combat transboundary haze, promote sustainable management practices, secure resources, develop policies, and enhance cross-sectoral cooperation (ASEAN 2024*a*). However, in Indonesia, the largest contributor to regional haze, the 2009 Forestry Law—which mandates imprisonment for those intentionally setting fires—has not been effectively enforced (Mai 2023).

resulting production patterns translate into environmental damages experienced by local and downwind countries.

On the trade side, we start from the sufficient-statistics framework of Arkolakis, Costinot and Rodríguez-Clare (2012), which provides a transparent way to measure real-income gains from trade using only observed domestic expenditure shares and estimated trade elasticities. When agricultural tariffs fall, domestic expenditure shares decline and production shifts toward the exporters that gain improved market access. This change in production does not require us to model full technologies or productivity distributions; instead, it is directly inferred from the ACR structure.

On the environmental side, the mechanism is that agricultural production in a Southeast Asian country i generates emissions whose effects are not confined to the location of origin. Atmospheric transport disperses these pollutants across national borders, exposing residents in downwind countries j regardless of whether the two countries engage in trade. To capture this spatial linkage, we employ a source–receptor matrix (E_{ij}) that summarizes the bilateral mapping from emissions generated in each origin to exposure experienced in each destination. This object compactly encodes the underlying transport dynamics and population distributions, and allows us to translate trade-induced shifts in the geography of production into corresponding changes in the geography of environmental damages. The welfare consequences of this exposure differ across countries. A unit of pollution arriving in country j may generate larger or smaller damages depending on its population density, baseline health conditions, or healthcare access. We capture this heterogeneity through a country-specific marginal damage parameter, denoted μ_j, which we borrow from environmental health research. Combining the transport matrix with the marginal damage parameters yields a simple structure: production changes in country i impose external costs on each downwind country j, proportional to how much pollution travels from i to j and how costly exposure is for residents of j.

Bringing together the trade and environmental channels yields a unified welfare frame-

work. Trade liberalization affects welfare through two components: it raises real income through the standard ACR mechanism, and it changes environmental damages by reallocating agricultural production across space. Because both effects are expressed in monetary terms, the net welfare impact is simply the difference between the real-income gain and the external cost borne by downwind countries.

3.1 Model Setup

We consider a world economy with N countries indexed by $i, j = 1, \ldots, N$ and two sectors indexed by $s \in \{A, N\}$, where A denotes agriculture and N denotes non-agriculture. Each country i is endowed with L_i units of labor. Labor is perfectly mobile across sectors within a country but immobile across countries. Let w_i denote the wage in country i and $y_i = w_i L_i$ its nominal income.

Preferences. Consumers in country j have homothetic preferences over sectoral composites with Cobb–Douglas expenditure shares $\alpha_j^s > 0$, $\sum_{s\in\{A,N\}} \alpha_j^s = 1$. Within each sector s, preferences are CES over country varieties with elasticity of substitution $\sigma_s > 1$. Utility in country j can be written as

$$U_j = \prod_{s\in\{A,N\}} (C_j^s)^{\alpha_j^s}, \qquad C_j^s = \left(\sum_{i=1}^{N} (c_{ij}^s)^{\frac{\sigma_s - 1}{\sigma_s}} \right)^{\frac{\sigma_s}{\sigma_s - 1}},$$

where c_{ij}^s denotes consumption of the variety produced in country i and consumed in country j in sector s. Let P_j^s denote the sectoral CES price index and P_j the overall Cobb–Douglas price index:

$$P_j^s = \left(\sum_{i=1}^{N} (p_{ij}^s)^{1-\sigma_s} \right)^{\frac{1}{1-\sigma_s}}, \qquad P_j = \prod_{s\in\{A,N\}} (P_j^s)^{\alpha_j^s},$$

where p_{ij}^s is the consumer price in j of the good produced in i in sector s.

Technology and Trade Costs. Production in each country-sector exhibits constant returns to scale and uses labor as the only primary factor. Let a_i^s denote the unit labor requirement in sector s in country i. The unit cost of production in i for sector s is then $c_i^s = w_i a_i^s$.

Trade frictions are captured by ad valorem tariffs on international shipments. Let $t_{ij}^s \geq 0$ denote the tariff rate imposed by country j on imports from country i in sector s.[7] The consumer price in j of the good produced in i in sector s is

$$p_{ij}^s = (1 + t_{ij}^s)\, c_i^s = (1 + t_{ij}^s)\, w_i a_i^s.$$

Equivalently, one can interpret $(1+t_{ij}^s)$ as an iceberg-type trade cost τ_{ij}^s, so that the canonical gravity structure is preserved while trade costs are empirically proxied by observed tariffs.

Gravity Structure. Expenditure in country j on sector s equals $\alpha_j^s y_j$. Given CES demand, the expenditure share in j allocated to producer i in sector s is

$$\lambda_{ij}^s = \frac{(p_{ij}^s)^{1-\sigma_s}}{\sum_{k=1}^N (p_{kj}^s)^{1-\sigma_s}},$$

where, from the pricing equation,

$$p_{ij}^s = (1 + t_{ij}^s)\, w_i a_i^s.$$

Substituting the tariff-based price into the gravity expression yields

$$\lambda_{ij}^s = \frac{[(1 + t_{ij}^s)\, w_i a_i^s]^{1-\sigma_s}}{\sum_{k=1}^N [(1 + t_{kj}^s)\, w_k a_k^s]^{1-\sigma_s}}.$$

[7] We abstract from other trade costs or normalize them to one, so that observed tariffs are the only source of variation in trade frictions that we exploit.

Let X_{ij}^s denote nominal spending in j on sector-s goods from i. Then

$$X_{ij}^s = \lambda_{ij}^s \, \alpha_j^s y_j.$$

Income and Trade Balance. Sectoral revenue in country i is

$$y_i^s = \sum_{j=1}^{N} X_{ij}^s = \sum_{j=1}^{N} \lambda_{ij}^s \alpha_j^s y_j,$$

and total income satisfies

$$y_i = \sum_{s \in \{A,N\}} y_i^s = w_i L_i.$$

Together, these conditions determine the general equilibrium vector of wages $\{w_i\}_{i=1}^N$ for any configuration of tariffs $\{t_{ij}^s\}$.

3.2 Real Income and ACR Sufficient Statistics

Let $\varepsilon_s = \sigma_s - 1$ denote the trade elasticity in sector s. Under the sufficient-statistics result of Arkolakis, Costinot and Rodríguez-Clare (2012), changes in real income depend only on the domestic expenditure shares λ_{jj}^s, regardless of the underlying micro structure of trade costs. In our setting, tariffs enter the model exclusively through their effect on prices and therefore on λ_{jj}^s.

Let $\widehat{Z}_{j,t} \equiv Z_{j,t}/Z_{j,0}$. Then real income in country j relative to the baseline is

$$\widehat{W}_{j,t} = \prod_{s \in \{A,N\}} \left(\frac{\lambda_{jj,t}^s}{\lambda_{jj,0}^s} \right)^{-\alpha_j^s/\varepsilon_s}. \tag{1}$$

A reduction in agricultural tariffs that lowers $\lambda_{jj,t}^A$ therefore raises $\widehat{W}_{j,t}$ through the standard gains-from-trade channel.

3.3 Agricultural Production, Emissions, and Transport

Agricultural production is the sole source of airborne particulate emissions. Let x_i^A denote agricultural output in country i, which equals its sectoral revenue:

$$x_i^A = y_i^A = \sum_{j=1}^{N} X_{ij}^A = \sum_{j=1}^{N} \lambda_{ij}^A \alpha_j^A y_j.$$

Since λ_{ij}^A is a function of tariff-inclusive prices $p_{ij}^A = (1 + t_{ij}^A) w_i a_i^A$, any change in tariffs mechanically reallocates agricultural production across origins.

Let χ_i denote emission intensity (tons of particulates per unit of output). Emissions from agriculture in country i satisfy

$$E_i = \chi_i x_i^A. \tag{2}$$

Emissions do not remain localized. Let $\Pi = (\pi_{ij})$ denote the source–receptor matrix, where $\pi_{ij} \in [0, 1]$ is the fraction of emissions generated in origin i that is ultimately inhaled in destination j. The matrix Π is estimated from atmospheric transport simulations and population exposure models and includes both domestic exposure ($\pi_{jj} > 0$) and transboundary transport ($\pi_{ij} > 0$ for $i \neq j$).

Exposure in country j is given by

$$\widetilde{E}_j = \sum_{i=1}^{N} \pi_{ij} E_i = \sum_{i=1}^{N} \pi_{ij} \chi_i x_i^A. \tag{3}$$

Thus, exposure depends jointly on the production allocation $\{x_i^A\}$ and the atmospheric transport structure encoded in Π.

3.4 External Damages and Welfare

Let $\mu_j > 0$ denote the marginal health damage (in monetary units) associated with one unit of exposure in country j. Given μ_j, the external cost borne by country j is

$$D_j = \mu_j \widetilde{E}_j = \sum_{i=1}^{N} \mu_j \pi_{ij} \chi_i x_i^A. \tag{4}$$

The term $\mu_j \pi_{ij} \chi_i$ represents the bilateral marginal external cost in j from agricultural production in i.

Welfare in j is defined as real income net of these external damages:

$$V_j = W_j - D_j.$$

In deviations from the baseline,

$$\Delta V_{j,t} = \Delta W_{j,t} - \Delta D_{j,t}.$$

3.5 Welfare Decomposition

Substituting (1) and (4), the change in welfare in country j between periods 0 and t is

$$\Delta V_{j,t} = \underbrace{\left[\prod_{s \in \{A,N\}} \left(\frac{\lambda^s_{jj,t}}{\lambda^s_{jj,0}} \right)^{-\alpha^s_j/\varepsilon_s} - 1 \right] W_{j,0}}_{\text{Gains from trade (ACR sufficient statistics)}} - \underbrace{\sum_{i=1}^{N} \mu_j \pi_{ij} \chi_i \left(x^A_{i,t} - x^A_{i,0} \right)}_{\text{External cost from tariff-induced reallocation of production}}. \tag{5}$$

The first term captures the conventional gains from trade driven by tariff-induced changes in domestic expenditure shares. The second term captures the environmental consequences of tariff-driven reallocation of agricultural production across origins, combined with atmo-

spheric transport and heterogeneous health vulnerabilities.

Whether agricultural trade liberalization raises or lowers welfare in country j depends on (i) how strongly tariffs affect production patterns, (ii) the spatial structure of pollution transport, and (iii) the magnitude of marginal damages μ_j.

3.6 Evaluation Paths

The welfare decomposition in (5) highlights that the effect of trade policy operates through two channels: (i) the real-income component summarized by changes in domestic expenditure shares, and (ii) the environmental component summarized by pollution exposure generated by the spatial allocation of agricultural production. We evaluate these mechanisms using both observed (ex-post) data and model-based (ex-ante) counterfactuals.

(1) Ex-Post (Descriptive). Given observed bilateral trade flows and expenditure data, we compute domestic expenditure shares in each sector directly as

$$\lambda^s_{jj,t} = \frac{X^s_{jj,t}}{\alpha^s_j y_{j,t}}.$$

The implied real-income change is

$$\widehat{W}^{\text{ex-post}}_{j,t} = \prod_{s\in\{A,N\}} \left(\frac{\lambda^s_{jj,t}}{\lambda^s_{jj,0}}\right)^{-\alpha^s_j/\varepsilon_s}.$$

Agricultural output is observed as

$$x^A_{i,t} = \sum_j X^A_{ij,t}, \qquad E_{i,t} = \chi_i x^A_{i,t},$$

and exposure and damages follow from

$$\widetilde{E}_{j,t} = \sum_i \pi_{ij} E_{i,t}, \qquad D_{j,t} = \mu_j \widetilde{E}_{j,t}.$$

The ex-post welfare series is therefore

$$\widehat{V}_{j,t}^{\text{ex-post}} = \widehat{W}_{j,t}^{\text{ex-post}} - \frac{D_{j,t} - D_{j,0}}{W_{j,0}}.$$

This descriptive measure captures the net effect of all forces in the data—tariff changes, productivity shocks, or demand shifts—and does not isolate the contribution of any specific policy.

(2) Ex-Ante (Counterfactual). To quantify the causal effect of trade policy, we compare the observed equilibrium to a counterfactual equilibrium generated by an alternative tariff schedule. Let $t_{ij,t}^{\text{real}}$ denote the observed tariff and $t_{ij,t}^{\text{cf}}$ the counterfactual value. This allows us to consider a wide range of policy experiments, including trade liberalization, trade wars, sector-specific tariff changes, or the removal of agricultural trade entirely.

For any counterfactual tariff vector $\{t_{ij,t}^{\text{cf}}\}$, we solve for the counterfactual general equilibrium wage vector w_t^{cf} satisfying

$$y_{i,t}^{\text{cf}} = w_{i,t}^{\text{cf}} L_i = \sum_{j=1}^{N} \sum_{s \in \{A,N\}} \lambda_{ij,t}^{s,\text{cf}} \alpha_j^s y_{j,t}^{\text{cf}},$$

where the counterfactual expenditure shares are

$$\lambda_{ij,t}^{s,\text{cf}} = \frac{\left[\left(1 + t_{ij,t}^{s,\text{cf}}\right) w_{i,t}^{\text{cf}} a_i^s\right]^{1-\sigma_s}}{\sum_{k=1}^{N} \left[\left(1 + t_{kj,t}^{s,\text{cf}}\right) w_{k,t}^{\text{cf}} a_k^s\right]^{1-\sigma_s}}.$$

Counterfactual agricultural output and emissions are

$$x_{i,t}^{A,\text{cf}} = \sum_j \lambda_{ij,t}^{A,\text{cf}} \alpha_j^A y_{j,t}^{\text{cf}}, \qquad E_{i,t}^{\text{cf}} = \chi_i x_{i,t}^{A,\text{cf}},$$

and exposure and damages follow from

$$\widetilde{E}^{\text{cf}}_{j,t} = \sum_i \pi_{ij} E^{\text{cf}}_{i,t}, \qquad D^{\text{cf}}_{j,t} = \mu_j \widetilde{E}^{\text{cf}}_{j,t}.$$

The real-income component of the causal effect is

$$\widehat{W}^{\text{ex-ante}}_{j,t} = \prod_{s\in\{A,N\}} \left(\frac{\lambda^{s,\text{real}}_{jj,t}}{\lambda^{s,\text{cf}}_{jj,t}} \right)^{-\alpha^s_j/\varepsilon_s},$$

and the environmental component is

$$\widehat{D}^{\text{ex-ante}}_{j,t} = D^{\text{real}}_{j,t} - D^{\text{cf}}_{j,t}.$$

(3) Total Welfare Effect. The total causal effect of a tariff change from $t^{\text{cf}}_{ij,t}$ to $t^{\text{real}}_{ij,t}$ is given by

$$\widehat{V}^{\text{ex-ante}}_{j,t} = \widehat{W}^{\text{ex-ante}}_{j,t} - \frac{D^{\text{real}}_{j,t} - D^{\text{cf}}_{j,t}}{W_{j,0}}. \tag{6}$$

Equation (6) applies to any pair of tariff schedules, enabling comparisons between observed trade, autarky, bilateral decoupling, agricultural-only liberalization, or any other policy regime.

4 Data

This section describes the data sources and the methodologies used to construct the datasets employed in this study. We compile a comprehensive panel covering fire activity, trade flows, agro-ecological suitability, environmental conditions, and socioeconomic data for 2003–2021. To study localized responses to national trade shocks, we construct a 0.1° global grid and harmonize all datasets to the grid level, yielding a high-resolution within-country panel for detailed spatial analysis of trade exposure and fire-induced pollution. The variables utilized in the main analysis are summarized in Table 1.

4.1 Fire Activities

FIRMS (Fire Information for Resource Management System) Our main outcome for fire activity comes from NASA's Fire Information for Resource Management System (FIRMS), which reports daily MODIS active-fire detections (Terra and Aqua) at 1 km resolution for 2003–2021.[8] Each detection includes geolocation, acquisition date, Fire Radiative Power (FRP, a proxy for combustion intensity), and quality flags. FIRMS also identifies persistent non-vegetation heat sources (for example, gas flares, industrial stacks, and volcanoes). We restrict the sample to vegetation fire detections by excluding persistent/static heat sources and water or invalid pixels, and we drop observations with confidence < 50 based on the quality flag. For the main analysis, we compute (i) the annual count of fire detections ("fire points") and (ii) the mean FRP per grid, aggregating daily detections to a 0.1° grid to obtain yearly measures of fire frequency and intensity suitable for linking to trade shocks. Figure 1 Panel A provides an example of the spatial distribution of the total number of fire activities across Southeast Asia in 2003. Most of the fires occur in the Southeast Asian mainland, indicating that land use practices in this region may contribute to the prevalence of fires.

We also construct a monthly FIRMS-based panel to distinguish land-clearing months from non-clearing months. Using this monthly dataset, we define fire activity during land-clearing months and fire activity during non-clearing months to explore whether trade-induced fires are concentrated in periods when burning is typically used for land preparation. FIRMS serves as our primary dataset, but it only reports active-fire hotspots rather than burned area or pollution emissions, and its time span is shorter than some alternatives. To check robustness and link fires to emissions, we also use complementary sources, including burned-area products and fire-emissions inventories.

[8] As the second satellite, Aqua, was launched in May 2002, data is available only from 2003 onward.

Fire Inventory from NCAR (FINN) The Fire Inventory from NCAR (FINN) dataset offers another important source of fire data. It provides monthly estimates of burn area, fire counts, and emissions (such as PM10, $PM_{2.5}$, and carbon emissions) from fire activities at a 0.1° resolution, covering the period from 2003 to 2020. This dataset is particularly useful for examining the environmental impact of agricultural fires, as it includes detailed information on burning areas and pollutant emissions associated with fire activities. We use the FINN dataset primarily for robustness checks to explore how trade-induced fire activity affects not only the burned areas but also the resulting pollution emissions.

4.2 Trade Measures

Our trade data is sourced from two main datasets: the UN Comtrade Database for export data and Teti (2025) for tariff data.

Export Data We obtain export data from the UN Comtrade Database, which provides detailed bilateral trade flows for goods classified under the Harmonized System (HS) at the 2-digit level, covering the period from 1995 to 2021. For our analysis, we define agricultural sectors using HS codes from 01 to 24, which encompass a wide range of agricultural products, including cereals, vegetables, fruits, and other processed food goods. We match this export data to grid-level panel data based on the export country name, allowing us to examine how agricultural trade shocks influence fire activity and land-use changes at a localized scale across different regions. In this context, the export value serves as a national-level shock, enabling us to assess the broader economic and environmental effects of trade on land-use patterns and fire activity in Southeast Asia.

Tariff Data We obtain tariff data from Teti (2025), which provides a comprehensive dataset on bilateral tariffs across countries from 1995 to 2021. This dataset includes detailed information on both Most Favored Nation (MFN) and preferential tariffs at the HS6 level. In our reduced-form analysis, we primarily focus on the MFN rate, treating Southeast

Asia as the exporter and aggregating all importers. To obtain the agricultural tariff rates, we calculate the simple average MFN tariff at the exporter level. This dataset enables us to assess how changes in agricultural tariff rates have influenced fire activity and agricultural expansion across different types of land in the region.

4.3 Crop Suitability Data

We measure agronomic potential using FAO/IIASA's Global Agro-Ecological Zones (GAEZ v4).[9] GAEZ evaluates each grid cell's climate, soils, and terrain against crop-specific requirements under assumed input/management levels (rainfed/irrigated) to produce suitability indices and attainable (potential) yields. For each crop–management setting, GAEZ computes an agro-climatic yield and applies reduction factors for thermal, moisture, soil, and terrain constraints to obtain a 0–100 *Suitability Index* (SI). SI values are grouped into ordered classes (Very suitable, Suitable, Moderately suitable, Marginally suitable, Very marginally suitable, Not suitable), which we convert to four bins in the analysis (very high, high, moderate, low/not suitable). These classes reflect binding biophysical constraints rather than current land use. Grids in the "not suitable" group have SI near zero because they face severe biophysical constraints (e.g., temperature or moisture limits, poor soils, steep slopes), so they are unlikely to be cultivated even if trade raises incentives. This makes them a credible reference group for within-country comparisons.

GAEZ also reports agro-climatic potential yields derived from eco-physiological crop models that incorporate radiation, temperature, and water balance. We use these potential yields to build a comparative suitability measure across grids and as a robustness check to our baseline classification. Figure 1 Panel B shows the distribution of land suitability across different levels, calculated based on the potential yield values for all crops in Southeast Asia. When compared with the spatial distribution of fire activities across Southeast Asia in 2003,

[9]GAEZ-based suitability and potential yields are standard in empirical trade and development work (Nunn and Qian 2011; Costinot, Donaldson and Smith 2016)

it is evident that most fires occur in areas with higher suitability, reinforcing the validity of the comparison.

4.4 Pollution Data

Our analysis incorporates the annual $PM_{2.5}$ dataset from the Atmospheric Composition Analysis Group at Washington University in St. Louis, covering the years 2003–2021 (Shen et al. 2024). This dataset provides high-resolution ($0.01^\circ \times 0.01^\circ$) global and regional surface-level $PM_{2.5}$ concentrations, which are sourced from satellite aerosol optical depth data, GEOS-Chem model outputs, and ground-based observations. We aggregate the mean values of $PM_{2.5}$ to a 0.1° resolution and use this dataset to investigate how fire activity impacts both local and transboundary pollution levels.

4.5 Land Use Data

We obtain land use data covering the period from 2001 to 2021, which provides detailed information on the percentage of cropland and forest coverage. The data is sourced from the MODIS Cropland Product (MCD12C1), and we have obtained it at a 0.1° resolution for all grids in the Southeast Asia (SEA) region. Cropland and forest coverage data enable us to examine land use changes across different types of land in response to trade shocks. Specifically, we use this data to investigate the underlying mechanisms driving the increase in fire points, examining whether trade shocks influence land use changes across different types of land and how these changes, particularly the expansion of agricultural areas, may directly impact fire activity.

4.6 Weather Controls

We use meteorological data from the Monthly Climate and Climatic Water Balance for Global Terrestrial Surfaces (TerraClimate) dataset, which provides monthly climate and

climatic water balance data for global terrestrial surfaces. Specifically, we utilize the Palmer Drought Severity Index (PDSI), precipitation accumulation, minimum temperature, and maximum temperature for each grid. We then calculate the annual mean values of these variables for the period from 2003 to 2021. These climate variables serve as control variables in our analysis. The data is sourced from the Google Earth Engine and includes daily measurements, which we aggregate to monthly and yearly levels at a 0.1° grid resolution.

To simulate the pollution trajectory for each grid, we also use meteorological data from the NCEP/NCAR Global Reanalysis dataset, published by the National Oceanic and Atmospheric Administration (NOAA). This dataset provides 6-hourly measurements at a 2.5° × 2.5° grid, including critical variables such as temperature, relative humidity, wind speed, and others. The HYSPLIT trajectory simulation model, which uses NCEP/NCAR data, enables us to simulate the potential movement of pollutants from fire activities across different regions. This model ensures consistency between our meteorological controls and the pollution trajectory predictions, helping us analyze the impact of fire activities on downwind pollution.

4.7 Socio-economic Data

Country Statistics We use socio-economic data on GDP, Agriculture Value Added, Industry Value Added, and Labor from the World Bank's database, covering the period from 1995 to 2021. The dataset is integrated into our model to characterize the income structure across various sectors, overall national income, and labor market conditions.

Gridded Population Data We obtain population data from the Gridded Population of the World, Version 4 (GPWv4) at the 30 arc-second grid level, which was subsequently aggregated to a 0.1-degree grid level. This population data allows us to estimate exposure to pollution originating from Southeast Asia (SEA) at the grid level. Pollution costs for each grid are then calculated based on population exposure, and the total pollution cost is

derived by summing the costs across all grids.

5 Agricultural Trade and Fire Activity in Southeast Asia

In this section, we investigate the impact of agricultural trade on fire activity in Southeast Asia, with a particular emphasis on the dynamic relationship between trade expansion and land-use changes. Land that is less suitable for crop cultivation is generally not utilized for agriculture, and as a result, it is less likely to be affected by trade shocks. In contrast, regions with higher agro-ecological suitability for agriculture are more likely to undergo land-use changes in response to agricultural trade expansion, especially through practices such as land clearing and the use of fire for crop production. Consequently, our primary focus is on examining the impact of agricultural exports on fire activity in areas that are more suitable for crop cultivation, as these regions are more likely to experience trade-induced changes in land use and fire activity.

5.1 Empirical Framework

We treat national-level trade shocks as exogenous to individual grids and focus on within-country variation in fire activity, exploiting differences in agro-ecological suitability across grids. The Global Agro-Ecological Zones (GAEZ) provide a suitability index for each grid worldwide, which reflects the land's potential for agricultural use based on a combination of climate, soil, and other environmental factors.[10]

Then, we use the suitability index to compare the fire response across grids with different

[10]The suitability index is divided into five categories: Not Suitable, Very Low Suitability, Low Suitability, Moderate Suitability, High Suitability, and Very High Suitability. We create five dummy variables, one for each suitability class. Each dummy variable equals 1 if a grid falls under the corresponding suitability class for any crop, and 0 otherwise. From GAEZ, we have data on 48 crops, including Alfalfa, Banana, Buckwheat, Barley, Biomass Sorghum, Cabbage, Carrot, Chickpea, Citrus, Cocoa, Coffee, Coconut, Cotton, Cowpea, Cassava, Flax, Foxtail Millet, Groundnut, Gram, Jatropha, Miscanthus, Maize, Oat, Oil Palm, Olive, Onion, Dry Pea, Phaseolus Bean, Pigeonpea, Pearl Millet, Dryland Rice, Reed Canary Grass, Wetland Rice, Rapeseed, Rye, Sunflower, Soybean, Sweet Potato, Sorghum, Sugarbeet, Sugarcane, Switchgrass, Tea, Tobacco, Tomato, Wheat, White Potato, and Yam.

levels of suitability. We define grids with very Low Suitability, not suitable, or low suitability for all crops as not suitable for cultivation and set them as the reference group, and we compare their agricultural fire activities with those of the other three suitability groups. In this analysis, we assume that grids with no suitability for any crop are unaffected by export shocks. The specification is as follows:

$$Fire_{cit} = \alpha + \sum_{k=1}^{3} \beta_k log(AgExport_{ct}) \times DSuit_i^k + \gamma' \mathbf{X}_{it} + \theta_c t + \tau_t + \pi_i + \varepsilon_{cit} \tag{7}$$

where $Fire_{cit}$ represents the outcome variable, indicating fire activity in grid i, country c, and year t, and the main outcome is the number of fire points. In the robustness check, we also use burning areas and pollutant emissions as the outcome variables. $\log(\text{AgExport}_{ct})$ captures the agricultural export value of country c in year t. $DSuit_i^k$ (k=1,2,3) are dummy variables indicating grids where at least one crop falls into moderate suitability, high suitability, and very high suitability, respectively. The other variables are defined in the previous section. We include country-year fixed effects θ_{ct} to compare the heterogeneous impact across grids within each country. Here, agricultural export is treated as a national shock, and local fire activity is unlikely to influence national exports, making trade shocks an exogenous source of variation across grids.

Furthermore, we include a set of grid-level controls, denoted by $\mathbf{X}_{ict}$. The model also includes year-fixed effects (τ_t), which control for macroeconomic shocks and policy changes that affect all grids in a given year, as well as grid-fixed effects (π_i) to account for time-invariant spatial characteristics that may influence fire activity, such as geographical features and baseline agricultural practices.

These controls include time-variant weather variables, such as precipitation, PDSI (Palmer Drought Severity Index), and temperature, to control for the influence of climatic factors on both agricultural productivity and fire activity. Additionally, we incorporate controls for interactions between year-fixed effects and pre-treatment grid-level characteristics to account

for baseline differences in fire activity and agricultural land use. Specifically, we include variables such as the number of fire points in each grid and whether the grid had cropland in the base year of 2003. These variables capture historical patterns of land use and fire activity, which may influence how these grids respond to trade shocks over time.

An increase in export value indicates a higher level of openness to trade, with tariffs serving as another important indicator of trade liberalization. Trade liberalization, often associated with tariff reductions, has significant implications for agricultural markets and environmental outcomes. Since export tariffs are primarily set by importing countries and received by exporters, local fire activities are unlikely to influence the tariff decisions made by importing nations. Therefore, we include the MFN (Most-Favored-Nation) tariff rates of importing countries as an additional variable of interest. The MFN tariff rate is an exogenous trade policy measure, as it is determined by the trade agreements and policies of the importing country, rather than by the exporting country's local conditions. Specifically, we use the agricultural export tariff to explore the heterogeneous effects of trade shocks and change the variable of interest from $log(AgExport_{ct})$ to $AgTariff_{ct}$ in Equation (7). $AgTariff_{ct}$ is the simple average MFN tariff across all agricultural products.

In this study, we use total agricultural export values for each country rather than focusing on crop-specific exports.[11] This allows us to capture the broader impacts of agricultural trade shocks, as changes in export patterns of more processed agricultural products—such as wheat flour or other higher-value derivatives—can influence land use and crop production at the grid level. Therefore, shocks in other agricultural sectors could lead to changes in land use decisions and agricultural expansion, which in turn could drive increased fire activity. For instance, a region suitable for growing wheat may experience shifts in production not only due to wheat exports but also due to the increases in exports of processed wheat products or other agricultural goods. This method accounts for the indirect effects of broader agricultural

[11]We also use crop-specific trade shocks and grid-crop level intensity treatments to construct the treatment exposure variable. Details of this approach can be found in the Appendix B.

activity, including sectors like livestock or forestry, on land use and potential fire risks.

5.1.1 Results

Panel A in Figure 2 displays the impact of agricultural export value on the grid-level yearly number of fire points. The impact is statistically significant in the high and very high suitability groups. A 1% increase in agricultural export value leads to an increase of 0.277 to 0.281 fire points per grid, compared to grids that are not suitable for agriculture; the mean value of fire points is 4.63; therefore, a 1% increase in agricultural export value could lead to a 6.5% increase in fire activities compared to grids that are not suitable.

Panel B in Figure 2 shows the impact of the simple average export MFN tariff on fire activity. A smaller tariff indicates a lower trade barrier. The results are similar to those for export value, with grids that fall into the more suitable and highly suitable categories showing a more significant impact compared to grids that are less suitable. Specifically, a smaller tariff is associated with an increase in fire activity, and as the suitability index increases, the effect becomes more pronounced. For suitable grids, a one-unit decrease in the tariff could lead to an increase in the number of fire points ranging from 0.0833 to 0.172 units (0.18%–0.37%).

In this analysis, it's important to note that crop-suitable grids might not be directly comparable to their counterparts due to differences in the baseline conditions of fire activity. Grids that are naturally more suitable for agriculture may already have higher baseline fire points, as these areas are often more forested due to favorable environmental conditions for plant growth. While these regions might experience more fires, it is crucial to distinguish between natural forest fires and human-induced agricultural fires. Forest fires, which are more common in areas with suitable conditions for crop growth, may occur more frequently in these regions, even in the absence of human intervention. Therefore, these grids could exhibit more fire activity due to forest fires rather than agricultural fires. To account for this, we control for the initial grid-level fire points by including year-fixed effects and grid-level

fire points as baseline controls in our model. This helps isolate the effect of trade on fire activity from the pre-existing fire conditions.

In addition, we will investigate whether, as trade volumes increase, crops-suitable areas experience a reduction in forest cover and a corresponding expansion of cropland in the next section. We will also examine whether this effect is more pronounced during land-clearing seasons, when agricultural practices such as slash-and-burn are more likely to occur.

5.2 Mechanism

We classify suitable grids as those with high and very high agro-ecological suitability, which exhibit greater agricultural potential. We then compare the dynamics of fire activity in these grids with those in grids with lower agro-ecological suitability. By doing so, we can assess whether regions with more favorable conditions for agriculture are more susceptible to land-use changes, such as agricultural expansion and deforestation, that drive fire activity. The empirical model is as follows:

$$Y_{cit} = \alpha + \beta log(AgExport_{ct}) \times Suit_i + \gamma' \mathbf{X}_{it} + \theta_c t + \tau_t + \pi_i + \varepsilon_{cit} \tag{8}$$

where $Suit_i$ are dummy variables indicating grids where at least one crop falls into the high or very high suitability group. Y_{cit} refers to different outcome variables, including changes in forest coverage, changes in cropland coverage, and the number of fire detections during both land clearing and non-land clearing periods. Other variables remain the same as in Equation (7).

To explore land-use shifts, we focus on two key variables: changes in cropland use and changes in forest cover. We primarily examine immediate shifts in land use, defined as the changes that occur between the current year and the previous year. Specifically, we define deforestation as the change in forest cover between the current year and the previous year. Similarly, changes in cropland coverage are measured in the same way, focusing on

year-on-year adjustments.

We hypothesize that regions with higher agro-ecological suitability will experience more extensive deforestation, as these areas are more likely to be targeted for agricultural expansion. The conversion of forested land to cropland, particularly in high-suitability areas, is often associated with the use of fire for land clearing, which contributes to an increase in fire points. An increase in cropland coverage signals agricultural land expansion, and we expect that areas with higher suitability for agriculture are more likely to experience greater cropland expansion in response to trade shocks. This expansion is likely to be accompanied by an increase in fire activity, as fire is commonly used to clear land for cultivation.

Furthermore, we differentiate between land-clearing periods and non-land-clearing periods to better understand the timing of fire activity. By classifying fire points according to these periods, we aim to identify whether fire activity is concentrated during specific times of the year, particularly those associated with agricultural land preparation and expansion. This distinction allows us to assess whether the observed increase in fire activity is predominantly driven by seasonal agricultural practices such as burning for land clearing, or whether other factors contribute to fire activity in these regions.

Results Table 2 presents the results of Equation (8). Column (1) shows the immediate effect on deforestation. As observed, grids with higher agricultural suitability experience a greater decrease in forest cover compared to grids with lower suitability. Specifically, a 1% increase in agricultural exports leads to a 0.112% decrease in forest cover in the short term.

Meanwhile, Column (2) reports the effects on cropland coverage. A 1% increase in agricultural exports results in a 0.07% increase in cropland coverage, indicating that trade expansion leads to agricultural land expansion. This shift in land use—where forest cover decreases and cropland increases—supports the argument that the land is being converted for agricultural purposes, particularly in areas with high agro-ecological suitability.

Columns (3) and (4) present the results for fire activity during the land-clearing and non-

land-clearing periods. During the land-clearing period, fire activity increases significantly ($p < 0.01$), with a 1% increase in agricultural exports leading to a 0.40-unit rise in the number of fire points. This significant increase in fire activity during the land-clearing period strongly suggests that the fires are primarily driven by agricultural land clearing, as fire is commonly used in this process to clear land for crops. In contrast, the effect during the non-land-clearing period is not statistically significant, reinforcing the notion that the fire activity observed is closely tied to agricultural practices, specifically land-clearing for crop cultivation.

5.3 Robustness Check

We have found that higher agricultural export values lead to an increased the frequency of agricultural fires in more suitable areas. Additionally, we observed that lower tariff barriers, as indicated by MFN tariff reductions, are associated with a rise in agricultural fires. In this subsection, we conduct a series of robustness checks to confirm these findings. Specifically, we carry out three types of robustness checks: (1) exploring alternative outcomes, (2) altering the definition of suitability, and (3) replacing the OLS regression model with the PPML regression model to further examine the intensive and extensive margins of the impact.

(i) Impact of Trade on Alternative Fire Outcomes In the baseline regression, we use the annual number of fire points as the outcome variable. However, this measure does not capture the potential effects on fire-induced pollution emissions or the burning areas. To address this limitation, we expand the analysis to assess not only the quantity of fire points but also the quality, specifically focusing on the intensity and strength of these fires. Therefore, we replace the outcome variable with various measures of fire-related pollution and intensity: CO_2 emissions, $PM_{2.5}$ emissions, the burning area, and the strength of the fire points (FRP), as described in Equation (8).

Table 3 reports the results, all of which are statistically significant at the 1% level. Column (1) highlights the significant impact of agricultural exports on the yearly burning

area in suitable regions. Specifically, a 1% increase in agricultural exports is associated with a 1.02% increase in the area burned in these areas. Columns (2) and (3) measure the impact on CO_2 and $PM_{2.5}$ emissions, respectively. Both columns show a positive and statistically significant relationship between agricultural exports and pollutant emissions. A 1% increase in agricultural exports corresponds to an increase of approximately 9.42×10^7 tons of CO_2 emissions and 2.15×10^4 tons of $PM_{2.5}$ emissions. Column (4) investigates the effect on the strength of the fire points (FRP), measured in megawatts (MW), and shows that a 1% increase in agricultural exports is linked to an increase of 0.7413 MW in fire intensity. This result supports the hypothesis that higher agricultural exports, particularly in areas with greater agricultural suitability, are associated with more intense fires. These findings collectively suggest that agricultural exports not only increase the frequency of fire points but also exacerbate pollution levels and the intensity of fires, underlining the environmental consequences of trade-driven agricultural expansion.

(ii) Extensive and Intensive Margins of Export Impact on Fire Activity. In this analysis, we examine both the extensive and intensive margin effects of agricultural exports on fire activity. The extensive margin measures whether a grid experiences any fire activity (i.e., whether there is at least one fire point in the grid), while the intensive margin measures the total number of fire points when a fire occurs in a grid. For the extensive margin, we use a binary variable indicating the presence or absence of fire activity in a given grid, and for the intensive margin, we use the total number of fire points in a grid where fire activity is observed. Additionally, we replace the OLS model with the PPML (Poisson Pseudo Maximum Likelihood) model to better handle count data and zero counts, while also allowing us to interpret the results as elasticities, providing more meaningful insights into the percentage change in fire points in response to agricultural exports.

Columns (1) and (2) in Table A1 present the results for the extensive and intensive margins, respectively, using OLS regression. Column (1) presents a result that is not sta-

tistically significant, while Column (2) shows that a 1% increase in agricultural exports is associated with a 0.00434% increase in the number of fire points. The results show that the effect primarily comes from the intensive margin, meaning that agricultural exports have more significant impact on the intensity of fire activity in areas where fires already occur, rather than simply affecting the likelihood of fire occurrence. This means that agricultural exports likely lead to more intensive land use in areas near or within existing cropland. As agricultural production expands, farmers may clear additional land through burning, often targeting areas that are adjacent to cropland. This also implies that the demand for straw burning could increase, as more crop residues are generated from the expanded agricultural activities, leading to more fires for land preparation or waste disposal. Column (2) shows that a 1% increase in agricultural exports is associated with a 0.0542% increase in the number of fire points.

In Columns (3) and (4), we switch to the PPML model and the extensive margin effect in Column (3) indicates that a 1% increase in agricultural exports is associated with a 0.00434% increase in the likelihood of fire occurrence, while the intensive margin effect in Column (4) shows that a 1% increase in agricultural exports corresponds to a 0.516% increase in the number of fire points. These results suggest that, in areas where fires do occur, higher agricultural exports lead to a significant increase in the number of fire points, with the effect being larger in the intensive margin.

(iii) Defining Suitability Based on the Potential Yield. Instead of using discrete suitability classes, we define suitability at the grid level using potential (attainable) yield from GAEZ as a continuous measure. Potential yield represents the average yield across all crops, measured in kilograms per hectare (kg/ha), and serves as an indicator of the agricultural potential of each grid.

$$Y_{cit} = \alpha + \beta log(AgExport_{ct}) \times PotentialYield_i + \gamma' \mathbf{X}_{it} + \theta_c t + \tau_t + \pi_i + \varepsilon_{cit} \qquad (9)$$

where $PotentialYield_i$ is the average potential yield among all crops for each grid. The exposure variable incorporates the relative potential yield for each grid, reflecting its agricultural potential compared to other grids. Grids with higher potential yields are assumed to be more likely to experience trade-induced agricultural shocks, making them more exposed to these shocks and their resulting environmental impacts, such as increased fire activity. Other variables remain the same as in Equation (7).

Table A2 reports the results from this robustness check. As shown in Column (1), the coefficient on the interaction term between agricultural exports and potential yield is positive and statistically significant. This suggests that in areas with each additional kilogram per hectare of potential yield, a 1% increase in agricultural exports is associated with a 0.0008% increase in the number of fire points. Similarly, Columns (2) to (4) show that the impact on other outcomes, such as emissions and burning areas, is also significant. These results further support the hypothesis that trade-induced agricultural expansion, particularly in areas with higher agricultural suitability as indicated by potential yield, is linked to increased fire activity and pollution emissions.

Across all robustness checks, coefficient magnitudes and inference remain stable, indicating that the main results are robust to alternative model specifications, data variations, and changes in the treatment definition.

6 Measuring the Environmental Externalities of Trade-induced Fires

In the previous section, we established that trade-induced fire activity increases in areas more suitable for crop cultivation. Given the pollution's ability to travel across regions, key questions arise: who suffers from these externalities, and what is the magnitude of the associated costs? In this section, we identify the areas impacted by agricultural fires and assess the environmental externalities linked to trade-induced fire activity. More importantly,

we evaluate how fire activities in one country affect the environmental quality of others, constructing an impact matrix between sources and receptors, which will be integrated into a model for later comparison with the welfare benefits of trade.

6.1 Identification of Downstream Areas

Transboundary air pollution is widely recognized as a major contributor to overall air pollution. To capture transboundary environmental and health effects, we identify the affected areas of the smoke induced by fires by using a state-of-the-art method, the Hybrid Single-Particle Lagrangian Integrated Trajectory model (HYSPLIT), which has been developed by the National Oceanic and Atmospheric Administration (NOAA) Air Resources Laboratory. HYSPLIT has been used in a variety of applications to describe atmospheric transport, dispersion, and deposition of pollutants (Lee, Wilson and Hsiang 2025; Heo, Ito and Kotamarthi 2025). By inputting meteorological and surface data, along with parameters for the pollutants and the location of the release source, the model can simulate the forward trajectories of pollutants from a given source over a specific time period.[12]

In this study, we simulate the daily pollution trajectories from 2003 to 2021, generating one-week forward trajectories for the center points of each grid in SEA countries. In total, we obtained 303,546,555 trajectories, which help identify receptor grids—locations impacted by pollution transported from source grids. Figure 3 illustrates examples of pollution trajectories originating from Southeast Asia. Panel A presents all pollution trajectories for March 2003, color-coded by transport days. The results indicate that pollution can travel as far as Australia, India, and even Russia within one week. Panel B shows the trajectories from Southeast Asia to Haikou during March 2003. The trajectories indicate that pollution from different locations reaches Haikou over varying transport days, implying that a single

[12]Meteorological data include wind fields, temperature, pressure, relative humidity, and surface characteristics such as land use, surface roughness, and terrain, which influence local wind patterns, mixing, and turbulence, all of which affect pollutant dispersion. Pollutant parameters include velocity, particle size, and other relevant factors. Further details are provided in the Appendix.

grid may experience fire-induced pollution from multiple sources at different times. Panel C provides two specific one-week trajectory examples originating from Myitkyina, Myanmar, on March 13 and March 14, 2003 and illustrates how pollution is transported within one week and how the trajectories can differ between days, even though the two days are close in time.

Based on these trajectories, we construct a grid-pair matrix that links each source grid with its corresponding receptor grids for each day of pollution transport.[13] This matrix represents the flow of pollutants from source grids to receptor grids over time. For each source grid, we calculate the probability of pollution reaching a receptor grid by using w days, using the following equation:

$$\text{ArriveProb}_{ijw} = \frac{1}{D_i} \sum_{d=1}^{D_i} \text{Arrive}_{ijw}, \tag{10}$$

where D_i is the total number of trajectory releases from source grid i over the entire sample period. The variable Arrive_{ijw} equals one if a trajectory originating from grid i reaches receptor grid j using w days, and 0 otherwise. Both D_i and Arrive_{ijw} are calculated over the sample period.

6.2 The Impact of Agricultural Fires on Pollution Levels

Model. Next, we will investigate how upstream agricultural fires affect downstream air pollution. Since different transport days may have varying impacts on downstream air pollution, for each receptor point, we aggregate the total upstream burning from all source points based on the number of days (forward days) it takes for the pollution to reach the receptor:

$$T_{jmw} = \sum_{i} \text{Arrive}_{ijmw} \cdot \text{Fire}_{i,m'}, \tag{11}$$

[13] We have 43,745 $0.1^\circ \times 0.1^\circ$grids in the SEA region, which serve as the source grids, and we identify approximately 2.7×10^5 grids that will be impacted by pollution originating from these regions.

where $\text{Fire}_{i,m'}$ is the number of fire points in cell i in year-month m' ($m' \in m-1, m$).[14] T_{jmw} is defined as the fire exposure at receptor grid j from fire activity transported over w days in year-month m. Due to the global satellite data providing the finest resolution of monthly $PM_{2.5}$ data, we match the monthly pollution levels at the receptor points with the corresponding upstream fire exposure.

Then, we could estimate the pollution effect of transported fires by using the following regression equation:

$$\text{PM}_{jm} = \alpha_j + \sum_{w=1}^{7} \beta_w T_{jmw} + \tau_m + \delta_w + \gamma' X_{jmw} + \varepsilon_{jmw}, \tag{12}$$

where PM_{jm} is the average $PM_{2.5}$ concentration in receptor cell j in month m, T_{jmw} is the fire exposure defined above. α_j are cell fixed effects, controlling for time-invariant grid-specific characteristics that could influence air quality in the grid j. The year–month fixed effects τ_m control for time-varying, month-specific factors that may affect $PM_{2.5}$ concentrations across all receptor grids during month m. δ_w represents forward-day fixed effects, accounting for potential non-linearities or temporal patterns in how pollution effects vary by the number of days (w) since the fire activity occurred. X_{jm} includes meteorological controls—such as temperature, relative humidity, and precipitation—for receptor grid j in month m, to isolate the effect of transported fire exposure from other environmental factors that can influence air quality.

Here, we estimate β_w using only the observations with positive exposure. As a result, β_w should be interpreted as a *conditional effect*, that is, the marginal impact of an additional upwind fire conditional on transport actually reaching receptor j.[15]

[14]Since pollution from the previous month may arrive at the receptor within one week, the pollution from source grids is measured as the $PM_{2.5}$ level in the releasing month.

[15]Estimating the conditional effect has several advantages: (i) The full sample contains a large mass of zero exposures, which would otherwise dominate the regression and obscure the signal; (ii) Separating conditional intensity from the probability of exposure provides a clearer decomposition into "strength" and "frequency" of transport events; (iii) Restricting to positive exposures mitigates attenuation bias from measurement error in near-zero values.

Results. Figure 4 shows the estimated impact of fire points on downwind $PM_{2.5}$ by transporting day ($w = 1, \ldots, 7$). The coefficients exhibit a monotonically decreasing trend with respect to w, with the effect on day 1 being the largest and diminishing to approximately one-fourth by day 7. This decline is consistent with how pollutants spread and fade in the atmosphere: dilution, deposition, and chemical changes reduce its impact over time. All coefficients are positive and precisely estimated, indicating that fires contribute to $PM_{2.5}$ at all lags, although the marginal influence diminishes quickly with transport time.

By construction, the coefficients, β_w, in Equation 12 is a conditional coefficient: it measures the marginal change in $PM_{2.5}$ at receptor j from one additional fire in source cell i, given that a fire occurs and arrives at receptor j after w days of transport. To translate a fire in i into pollution at j, two conditions must hold: (i) receptor j experiences a positive w-day fire exposure, $\Pr(T_{jw} > 0)$; and (ii) the fire-induced smoke travels from i to j using day w with the corresponding arrival probability, ArriveProb_{ijw}. For cost–benefit accounting, we convert this conditional effect into an unconditional expected effect by weighting β_w by these two probabilities for each transporting day w to construct a source–to–receptor impact matrix. The marginal change in $PM_{2.5}$ at receptor j in month m caused by one additional fire in source i is given by

$$\rho_{ij} = \frac{\partial \text{PM}_j}{\partial \text{Fire}_i} = \sum_{w=1}^{7} \beta_w \cdot \Pr(T_{jw} > 0) \cdot \text{ArriveProb}_{ijw}, \tag{13}$$

where $\Pr(T_{jw} > 0)$ is estimated empirically as the fraction of months in which receptor j receives a positive exposure from transporting day w.[16] ArriveProb_{ijw} denotes the average transport probability from source i to receptor j using transporting day w and has been defined above, calculated over the sample period. This formulation ensures that ρ_{ij} cap-

[16] $\Pr(T_{jw} > 0)$ is estimated over the sample period, where $\Pr(T_{jw} > 0)$ is defined as: $\Pr(T_{jw} > 0) = \frac{Day(\text{Arrive}_{jw}>0)}{TotalDays}$, where $Day(\text{Arrive}_{jw} > 0)$ represents the number of days during which the exposure to w-days-before fire in grid j is greater than zero, and $TotalDays$ is the total number of days in the sample period (2003—2021) for which trajectory data is available.

tures both the intensity of fire-driven pollution when transport occurs and the likelihood of such transport events. Figure A9 illustrates how fires in other SEA grid cells influence air pollution in a specific grid, in this case, Singapore, representing the spatial effect ρ_{ij} with $j =$ Singapore. The effect is larger for grids closer to Singapore, with larger values of ρ_{ij}.

It needs to be noted that we exclude grid cells with active fire occurrences and interpret the first-day effect as a localized impact. While this approach may result in an underestimation of the true local effect, it is necessary to reduce the endogeneity bias that would arise from directly estimating the effect within the fire-origin cells.

The impact factor between source grid i and receptor grid j, denoted as ρ_{ijw}, quantifies the effect of fires in the SEA region on both local ($i = j$) and downstream air quality. Specifically, it represents how fire activity in grid i influences pollution levels in receptor grid j. By aggregating across all source grids, $\sum_i \rho_{ij}$, we can measure the total impact from external sources, which indicates changes in pollution in receptor grid j resulting from a unit increase in fire activity across all source grids. Additionally, ρ_{ij} helps us assess the contribution to downwind regions of each source grid i by aggregating it over all receptor grids, $\sum_j \rho_{ij}$. This captures the total increase in pollution caused by a unit increase in fire activity at source grid i. ρ_{ij} quantifies the transboundary impact of fire from grid i on pollution levels in receptor grid j, and in the next section, we will use the parameter to estimate the pollution cost of trade-induced fire activities, as it provides a sufficient statistic linking an additional fire in each source grid to the resulting increase in $PM_{2.5}$ exposure in each receptor grid.

6.3 The Pollution Costs of Agricultural Exports

We decompose pollution damages into three components: (i) trade shocks alter fire activity at source grids (Section 5); (ii) the pollution cost of per fire activity; (iii) the trade shock, which could be an increase in export value or a reduction of tariff.

We compute the pollution cost of international trade in three steps. First, we obtain the

trade-induced change in fire points at each source grid by using Equation (7). Second, we map that change into receptor-specific $PM_{2.5}$ increments using our transport estimates for all connected source–receptor pairs, and monetize those $PM_{2.5}$ increments at each receptor using the elasticity of pollution on mortality and morbidity rates from the literature. Third, incorporating the trade shock, we then aggregate: summing over source grids gives the total burden borne by each receptor (domestic plus transboundary), while summing over receptor grids gives the domestic and transboundary damages caused by each source (or by a source country). Accordingly, the pollution cost attributable to fires in source grid i and borne by the receptor grid j is given by:

$$\text{Pollution Cost}_j = \sum_i \Gamma_i \times \Delta \log(\text{AgExport}_c) \times \Lambda_{ij} \tag{14}$$

where Γ_i denotes the grid-level marginal effect of agricultural exports on fire points—that is, the increase in the number of fires in grid i associated with a 1% increase in national agricultural exports. In the previous subsection, we estimated these semi-elasticities using interactions between $\log(\text{AgExport}_{ct})$ and agro-ecological suitability dummies (Equation (7)). Using the estimated coefficients and the suitability class of grid i, we obtain:

$$\Gamma_i \;=\; \sum_{k=1}^{3} \beta_k \, DSuit_i^k, \tag{15}$$

where $DSuit_i^k \in \{0, 1\}$ ($k \in \{1$ (Moderate), 2 (High), 3 (Very High)$\}$) indicates the suitability class for each grid i and the detailed definition could be found in Section 5. β_k is the corresponding coefficient in Figure 2, Panel A.

The parameter Λ_{ij} denotes the pollution cost at receptor grid j caused by an additional fire in source grid i. From the previous section, we have estimated the source–receptor linkage ρ_{ij}, which maps a unit increase in burning at i into $PM_{2.5}$ at j. Monetized damages at j depend on the valuation of pollution (mortality and morbidity responses) and the exposed population. Let μ_j be the monetary cost per unit $PM_{2.5}$ at j (health-response coefficients $\times$

population). The parameter Λ_{ij} could be calculated by the following equation:

$$\begin{aligned}\Lambda_{ij} = &\quad \mu_j \cdot \rho_{ij} \\ = &\quad VSL_c \cdot \frac{\partial \text{Mortality}_j}{\partial \text{PM}_j} \cdot \text{Pop}_j \cdot \rho_{ij} + \underbrace{\frac{\partial \text{Health Care Cost}_j}{\partial \text{PM}_j} \cdot \text{Pop}_j \cdot \rho_{ij}}_{\text{Morbidity Cost}} \end{aligned} \tag{16}$$

$$\underbrace{\qquad\qquad\qquad\qquad}_{\text{Mortality Cost}}$$

where VSL_c refers to the Value of Statistical Life for country c, and Pop_j is the population residing in receptor grid j. $\frac{\partial \text{Mortality}_j}{\partial \text{PM}_j}$ is the causal effect of $\text{PM}_{2.5}$ on mortality rate, which was obtained from He, Liu and Zhou (2020). $\frac{\partial \text{Health Care Cost}_j}{\partial \text{PM}_j}$ is the coefficient of $\text{PM}_{2.5}$ exposure to morbidity cost, obtained from Barwick et al. (2024). Both link this increase in pollution to the corresponding health costs in receptor grid j. In Equation (**??**), Λ_{ij} represents either the morbidity burden (i.e., the number of additional health events such as hospital visits) or, when combined with monetary valuation, the associated health cost received by cell j and attributable to one additional fire in cell i. ρ_{ij} measures the marginal effect of one transport-weighted fire on $\text{PM}_{2.5}$ concentration at transporting day w.

In this research, we focus on estimating the environmental externalities of trade—namely, health costs arising from fire-driven $\text{PM}_{2.5}$ pollution. Other potential health benefits of trade (e.g., via higher incomes, improved health-care access, or technology diffusion) are not the focus of this paper and are therefore left out of our estimates. Importantly, our externality measure should be viewed as a lower bound on total environmental damages: we (i) isolate only the fire–$\text{PM}_{2.5}$ pathway (excluding non-fire emissions and other pollutants such as ozone), (ii) exclude origin cells with active fires to mitigate endogeneity, which likely attenuates near-source impacts, (iii) aggregate to monthly exposure, which smooths peaks, and (iv) rely on satellite-based $\text{PM}_{2.5}$ with classical measurement error. In the next section, we combine this lower-bound damage estimate with a standard ACR-style measure of the gains from trade, reporting both gross gains and net gains after integrating the monetized

pollution costs into a general equilibrium model.

Results We simulate the scenario where the agricultural export value in the entire SEA region increases by 1 USD to calculate the associated pollution cost from trade-induced fires using Equation (14).[17]. The results are shown in Figure 5. Panel A presents the pollution costs in SEA countries, breaking down the costs into domestic and transboundary pollution sources. Indonesia incurs the highest health cost, at 0.0423 (0.0302, 0.0537) USD, with 94% of the pollution coming from domestic fires. However, for other countries, particularly those with lower levels of development, transboundary pollution plays a more significant role. Figure A11 illustrates the share of transboundary pollution costs for each country in SEA. While Laos and Timor-Leste have lower overall pollution costs compared to Indonesia, transboundary pollution accounts for 83% and 64%, respectively. More importantly, Singapore, a highly urbanized city-state with minimal agricultural land, has 100% of its pollution cost coming from outside the country, making it a receptor of transboundary pollution. Additionally, Thailand and Vietnam bear the second and third highest costs, with transboundary pollution contributing 30%-50% of their total pollution costs.

Figure 5 Panel B illustrates the spatial distribution of pollution costs resulting from a 1 USD increase in agricultural export value. The impact decreases as the distance from the SEA region increases. Pollution from trade-induced fires in SEA affects a broad range of countries, extending from India to Japan in the east, and from Australia to Russia in the south and north, respectively. When the agricultural export value increases by 1 USD, the total global pollution cost is 0.115 USD. Figure A10 presents the pollution costs for all non-SEA countries and regions. In total, 31 countries and regions are affected by trade-induced fires. China incurs the highest pollution cost due to its geographical proximity to SEA and its large population. India and Japan also experience substantial costs. Overall, the spatial

[17]We calculate the pollution cost by applying the known 1% impact and then adjust it by dividing by the average total agricultural export value across the SEA region for the sample period (2003–2021).

distribution of pollution costs highlights the significant cross-border impact of trade-induced fires, particularly on neighboring and economically significant countries.

7 Model Application and Counterfactual Analysis

7.1 From Theory to the Data

The quantitative model developed in Section 3 requires four empirical inputs in order to map theory to data: (i) bilateral ad-valorem tariff schedules that determine changes in iceberg trade costs; (ii) sector-specific trade elasticities; (iii) bilateral expenditure shares across agriculture and non-agriculture; and (iv) an exposure–response system that links agricultural emissions to downwind pollution damages through the transport matrix $\Pi = [\pi_{od}]$ and the country-specific health–damage parameter μ_d.

The data on $\hat{\tau}_{od}^{j}$ measure how changes in bilateral tariffs alter trade costs between trading partners. These tariff schedules are observed by product and partner country and can be aggregated into sectoral trade costs for agriculture and non-agriculture. Section 4 describes the data sources and aggregation procedures used to construct bilateral ad-valorem tariff equivalents between countries. Because other trade frictions such as distance or language are time-invariant, tariff variation provides the main source of identifying variation for our counterfactual analysis. The sector-specific elasticities θ^j govern the responsiveness of bilateral trade flows to changes in trade costs. Following the quantitative trade literature, we take θ^A and θ^N from Simonovska and Waugh (2014); Caliendo and Parro (2015); Costinot and Rodríguez-Clare (2014). Agricultural goods typically display lower elasticities due to higher differentiation and transport frictions, whereas non-agricultural goods exhibit larger elasticities consistent with greater substitutability.

We use observed bilateral expenditure shares λ_{od}^{j} as the baseline allocation of country d's spending across origins o. These shares are obtained from World Bank Indicators and correspond exactly to the CES structure in the multi-sector model. The trade elasticity θ^j

represents the responsiveness of bilateral trade flows to changes in trade costs, holding wages and prices fixed.

Agricultural emissions and cross-border transport. A central innovation of the model is the mapping from agricultural trade to environmental exposure. Let E_o denote the annual mass of agricultural-fire emissions produced in country o. The transport matrix π_{od} measures the expected increase in annual-average $PM_{2.5}$ concentration in receptor d generated by one unit of emissions in origin o. In practice, π_{od} is constructed by aggregating grid-to-grid transport probabilities from a chemistry–transport model (i.e., HYSPLIT) and weighting receptor grids by population.

Health damage scaling parameter. To map exposure into welfare, the model uses a multiplicative penalty:

$$\Psi_d \;=\; \exp\Big(-\mu_d \left[\widetilde{E}_d^{\text{real}} - \widetilde{E}_d^{\text{cf}}\right]\Big),$$

where μ_d is calibrated so that the welfare loss from additional exposure matches monetized damages.

7.2 Results: Global Distribution of Trade Gains and Environmental Costs

Figure 6 summarizes the global distribution of gains and environmental costs from agricultural trade with SEA, comparing observed 2021 trade to a counterfactual scenario in which SEA's agricultural exports face prohibitive trade costs.

Almost all countries experience positive gains from SEA's participation in global agricultural markets. Large economies, such as China and the United States, obtain substantial improvements in real income. Even geographically distant countries capture efficiency gains through expanded sourcing options and lower food prices. These patterns are consistent with standard predictions from quantitative trade models. In sharp contrast, the environmental costs generated by transboundary pollution exhibit a highly uneven spatial distribution.

Countries located downwind of SEA, particularly China, experience large losses in environmental costs. Because China's population is exceptionally large, the exposure scales up markedly, resulting in a sizable welfare penalty via the damage. In our baseline calibration, the implied environmental cost exceeds 10% of GDP, which largely offsets trade gains. We find Singapore and other small coastal economies face minimal external exposure. Their limited land area, low population, and atmospheric dispersion patterns jointly imply very small possibilities of being affected by agricultural fires, allowing them to enjoy substantial trade gains while incurring negligible pollution damages. Similarly, distant countries such as the United States and those in Europe experience almost pure gains, benefiting from market integration without bearing any significant environmental externalities.

Taken together, these results reveal a pronounced spatial inequity in the welfare consequences of international trade. The benefits of SEA's openness accrue globally, but the environmental costs are concentrated among a handful of populous downwind nations. Conventional trade analysis, which focuses solely on changes in real income, would overlook this asymmetry entirely. Our integrated trade–environment framework shows that atmospheric transport can fundamentally reshape the distribution of welfare gains, and that trade liberalization may impose substantial hidden costs on pollution-receiving countries.

8 Conclusion

Environmental externalities are central to evaluating trade policy. Developing countries with comparative advantage in pollution-intensive industries face the risk of severe environmental degradation unless appropriate policies are implemented (Lee and Roland-Holst 1997). Yet quantifying these externalities—particularly when pollution crosses borders—remains a significant empirical challenge. This paper addresses this gap by developing a framework that explicitly incorporates international pollution costs into trade welfare analysis. Applied to Southeast Asian agricultural exports, our analysis reveals that each dollar of export growth

generates $0.11 in global health damages from fire-induced air pollution, with costs dispersed across more than 40 countries. These estimates provide an empirical foundation for designing policies that internalize cross-border environmental externalities.

The transboundary nature of pollution presents a coordination problem: benefits concentrate in exporting countries while costs disperse internationally. The Coase theorem suggests that, with well-defined property rights and low transaction costs, affected parties could bargain to efficient outcomes (Coase 1960). This logic implies that countries could negotiate to internalize externalities—through compensation, technology transfers, or coordinated standards. However, Coase's conditions rarely hold in practice. Property rights over transboundary air quality remain ambiguous, transaction costs are high when dozens of countries with asymmetric stakes must coordinate, and enforcement requires institutional capacity that often exceeds what regional organizations possess. ASEAN's experience illustrates these challenges: despite the 2002 Agreement on Transboundary Haze Pollution, implementation has been limited by sovereignty concerns, monitoring difficulties, and misalignment between national incentives and regional commitments. A fundamental obstacle to both source-based regulation and international bargaining is the absence of credible cost estimates. Pigouvian taxes or subsidies at the pollution source require knowing the marginal damage to set efficient rates, while compensatory transfers from beneficiaries to victims require agreement on total damages. Our framework addresses this gap by quantifying health costs across affected populations and linking them to specific pollution sources. These estimates provide the empirical basis for calibrating source-country interventions and establishing bargaining parameters for cross-border compensation.

References

Akerman, Anders, Rikard Forslid, and Ossian Prane. 2024. "Imports and the CO2 emissions of firms." *Journal of International Economics*, 152: 104004.

Arkolakis, Costas, Arnaud Costinot, and Andrés Rodríguez-Clare. 2012. "New Trade Models, Same Old Gains?" *American Economic Review*, 102(1): 94–130.

ASEAN. 2002. "ASEAN Agreement on Transboundary Haze Pollution."

ASEAN. 2024*a*. "Haze." Accessed February 12, 2024.

ASEAN. 2024*b*. "Launch of the second ASEAN haze-free roadmap (2023-2030) and policy dialogue on strategies and actions for achieving a haze-free Southeast Asia." Accessed February 12, 2024.

Azmi, Hadi. 2025. "Malaysian students allowed to stay at home as annual haze crisis begins."

Barwick, Panle Jia, Shanjun Li, Deyu Rao, and Nahim Bin Zahur. 2024. "The healthcare cost of air pollution: evidence from the world's largest payment network." *Review of Economics and Statistics*, 1–52.

BBC. 2013. "Indonesian Forest Fires 'Worst in 16 Years' - Reports." Accessed: 2025-11-05.

Bombardini, Matilde, and Bingjing Li. 2020. "Trade, Pollution and Mortality in China." *Journal of International Economics*, 125: 103321.

Borgschulte, Mark, David Molitor, and Eric Yongchen Zou. 2024. "Air pollution and the labor market: Evidence from wildfire smoke." *Review of Economics and Statistics*, 106(6): 1558–1575.

Caliendo, Lorenzo, and Fernando Parro. 2015. "Estimates of the Trade and Welfare Effects of NAFTA." *The Review of Economic Studies*, 82(1): 1–44.

Carreira, Igor, Francisco Costa, and Joao Paulo Pessoa. 2024. "The deforestation effects of trade and agricultural productivity in Brazil." *Journal of development economics*, 167: 103217.

Cherniwchan, Jevan, Brian R. Copeland, and M. Scott Taylor. 2017. "Trade and the Environment: New Methods, Measurements, and Results." *Annual Review of Economics*, 9(1): 59–85.

Cheung, Chun Wai, Guojun He, and Yuhang Pan. 2020. "Mitigating the Air Pollution Effect? The Remarkable Decline in the Pollution-Mortality Relationship in Hong Kong." *Journal of Environmental Economics and Management*, 101: 102316.

Clausing, Kimberly A., and Catherine Wolfram. 2023. "Carbon Border Adjustments, Climate Clubs, and Subsidy Races When Climate Policies Vary." *Journal of Economic Perspectives*, 37(3): 137–162.

Coase, Ronald H. 1960. "The Problem of Social Cost." *Journal of Law and Economics*, 3: 1–44.

Copeland, Brian R. 2008. "The Pollution Haven Hypothesis." In *Handbook on Trade and the Environment.* , ed. Kevin P. Gallagher, Chapter 2.7, 60–70. Cheltenham, UK and Northampton, MA, USA:Edward Elgar Publishing.

Copeland, Brian R., and M. Scott Taylor. 2003. *Trade and the Environment: Theory and Evidence.* Princeton, NJ:Princeton University Press.

Copeland, Brian R., and M. Scott Taylor. 2004. "Trade, Growth, and the Environment." *Journal of Economic Literature*, 42(1): 7–71.

Costinot, Arnaud, and Andrés Rodríguez-Clare. 2014. "Trade Theory with Numbers: Quantifying the Consequences of Globalization." In *Handbook of International Economics.* Vol. 4, , ed. Gita Gopinath, Elhanan Helpman and Kenneth Rogoff, 197–261. Elsevier.

Costinot, Arnaud, Dave Donaldson, and Cory Smith. 2016. "Evolving comparative advantage and the impact of climate change in agricultural markets: Evidence from 1.7 million fields around the world." *Journal of Political Economy*, 124(1): 205–248.

Cristea, Anca, David Hummels, Laura Puzzello, and Misak Avetisyan. 2013. "Trade and the greenhouse gas emissions from international freight transport." *Journal of environmental economics and management*, 65(1): 153–173.

Dasgupta, Partha S., and Paul R. Ehrlich. 2013. "Pervasive Externalities at the Population, Consumption, and Environment Nexus." *Science*, 340(6130): 324–328.

Devex. 2019. "Balancing development goals to fix Southeast Asia's haze." Accessed: 2025-11-05.

Dicken, Peter. 2015. *Global Shift: Mapping the Changing Contours of the World Economy.* . 7th ed., New York:Guilford Press.

Dipoppa, Gemma, and Saad Gulzar. 2024. "Bureaucrat incentives reduce crop burning and child mortality in South Asia." *Nature*, 634: 1125–1131.

Duan, Yuwan, Ting Ji, Yi Lu, and Siying Wang. 2021. "Environmental Regulations and International Trade: A Quantitative Economic Analysis of World Pollution Emissions." *Journal of Public Economics*, 203: 104521.

Du, Xinming, Lei Li, and Eric Zou. 2024. "Trade, Trees, and Lives." National Bureau of Economic Research.

Ederington, Josh, Arik Levinson, and Jenny Minier. 2005. "Footloose and Pollution-Free." *The Review of Economics and Statistics*, 87(1): 92–99.

Fontagné, Lionel, and Katheline Schubert. 2023. "The Economics of Border Carbon Adjustment: Rationale and Impacts of Compensating for Carbon at the Border." *Annual Review of Resource Economics*, 15: 389–424.

Fowlie, Meredith, Mar Reguant, and Stephen P. Ryan. 2016. "Market-Based Emissions Regulation and Industry Dynamics." *Journal of Political Economy*, 124(1): 249–302.

Garg, Teevrat, Maulik Jagnani, and Hemant K Pullabhotla. 2024. "Rural roads, farm labor exits, and crop fires." *American Economic Journal: Economic Policy*, 16(3): 420–450.

Gutiérrez, Emilio, and Kensuke Teshima. 2018. "Abatement expenditures, technology choice, and environmental performance: Evidence from firm responses to import competition in Mexico." *Journal of Development Economics*, 134: 215–231.

Hanson, Gordon H. 2012. "The Rise of Middle Kingdoms: Emerging Economies in Global Trade." *Journal of Economic Perspectives*, 26(2): 41–64.

He, Guojun, Tong Liu, and Maigeng Zhou. 2020. "Straw burning, PM2. 5, and death: Evidence from China." *Journal of Development Economics*, 145: 102468.

Heo, Seonmin Will, Koichiro Ito, and Rao Kotamarthi. 2025. "International Spillover Effects of Air Pollution: Evidence from Mortality and Health Data Unavailable." *The Review of Economics and Statistics*, 1–45.

Jia, Ruixue, and Hyejin Ku. 2019. "Is China's Pollution the Culprit for the Choking of South Korea? Evidence from the Asian Dust." *The Economic Journal*, 129(624): 3154–3188.

Jong, Hans Nicholas. 2025. "NASA Satellites Show Surge in Indonesia Hotspots as 2025 Fires Send Smoke to Malaysia."

Kellenberg, Derek. 2012. "Trading Wastes." *Journal of Environmental Economics and Management*, 64(1): 68–87.

Kellenberg, Derek K. 2009. "An Empirical Investigation of the Pollution Haven Effect with Strategic Environment and Trade Policy." *Journal of International Economics*, 78(2): 242–255.

Larch, Mario, and Joschka Wanner. 2017. "Carbon tariffs: An analysis of the trade, welfare, and emission effects." *Journal of International Economics*, 109: 195–213.

Lee, Hiro, and David Roland-Holst. 1997. "The Environment and Welfare Implications of Trade and Tax Policy." *Journal of Development Economics*, 52(1): 65–82.

Lee, Jaecheol, Andrew J Wilson, and Solomon M Hsiang. 2025. "Empirically Distinguishing Health Impacts of Transboundary and Domestic Air Pollution in Mixture." National Bureau of Economic Research.

Mai, Lauren. 2023. "Extinguishing a Point of Contention: Examining Transboundary Haze in Southeast Asia." *The Diplomat*. Accessed February 13, 2024.

Nunn, Nathan, and Daniel Qian. 2011. "The Potato's Contribution to Population and Urbanization: A New Perspective on the Columbian Exchange." *The Quarterly Journal of Economics*, 126(2): 751–794.

Rangel, Marcos A, and Tom S Vogl. 2019. "Agricultural fires and health at birth." *Review of Economics and Statistics*, 101(4): 616–630.

Reuters. 2023. "What's causing the chronic haze across Southeast Asia?"

Rodrigue, Joel, Dan Sheng, and Yong Tan. 2024. "Exporting, abatement, and firm-level emissions: Evidence from China's accession to the WTO." *Review of Economics and Statistics*, 106(4): 1064–1082.

Shapiro, Joseph S. 2016. "Trade Costs, CO_2, and the Environment." *American Economic Journal: Applied Economics*, 8(4): 220–252.

Sheldon, Tamara L, and Chandini Sankaran. 2017. "The impact of Indonesian forest fires on Singaporean pollution and health." *American Economic Review*, 107(5): 526–529.

Shen, Siyuan, Chi Li, Aaron Van Donkelaar, Nathan Jacobs, Chenguang Wang, and Randall V Martin. 2024. "Enhancing global estimation of fine particulate matter concentrations by including geophysical a priori information in deep learning." *Acs Es&T Air*, 1(5): 332–345.

Shi, Xin, and Meng Zhang. 2023. "Waste import and air pollution: Evidence from China's waste import ban." *Journal of Environmental Economics and Management*, 121: 102777.

Simonovska, Ina, and Michael E. Waugh. 2014. "The Elasticity of Trade: Estimates and Evidence." *Journal of International Economics*, 92(1): 34–50.

Tanaka, Shinsuke, Kensuke Teshima, and Eric Verhoogen. 2022. "North-South displacement effects of environmental regulation: The case of battery recycling." *American Economic Review: Insights*, 4(3): 271–288.

Teti, Feodora. 2025. "Missing Tariffs." *Working Paper*.

Vongruang, Patipat, and Sittichai Pimonsree. 2020. "Biomass burning sources and their contributions to PM10 concentrations over countries in mainland Southeast Asia during a smog episode." *Atmospheric Environment*, 228: 117414.

Wang, Xiaoxi, Meng Xu, and Kevin Chen. 2025. "Internalizing Externalities through Ecological Compensation: Evidence from Trans-Boundary Water Pollution in China." *Journal of Environmental Economics and Management*, 133: 103200.

Zheng, Haotian, Di Wu, Shuxiao Wang, Xiangdong Li, Ling N Jin, Bin Zhao, Shengyue Li, Yisheng Sun, Zhaoxin Dong, Qingru Wu, et al. 2025. "Control of toxicity of fine particulate matter emissions in China." *Nature*, 643(8071): 404–411.

Zhu, J, X Xia, H Che, J Wang, J Zhang, and Y Duan. 2016. "Study of aerosol optical properties at Kunming in southwest China and long-range transport of biomass burning aerosols from North Burma." *Atmospheric Research*, 169: 237–247.

Zivin, Joshua Graff, Tong Liu, Yingquan Song, Qu Tang, and Peng Zhang. 2020. "The unintended impacts of agricultural fires: Human capital in China." *Journal of Development Economics*, 147: 102560.

9 Tables and Figures

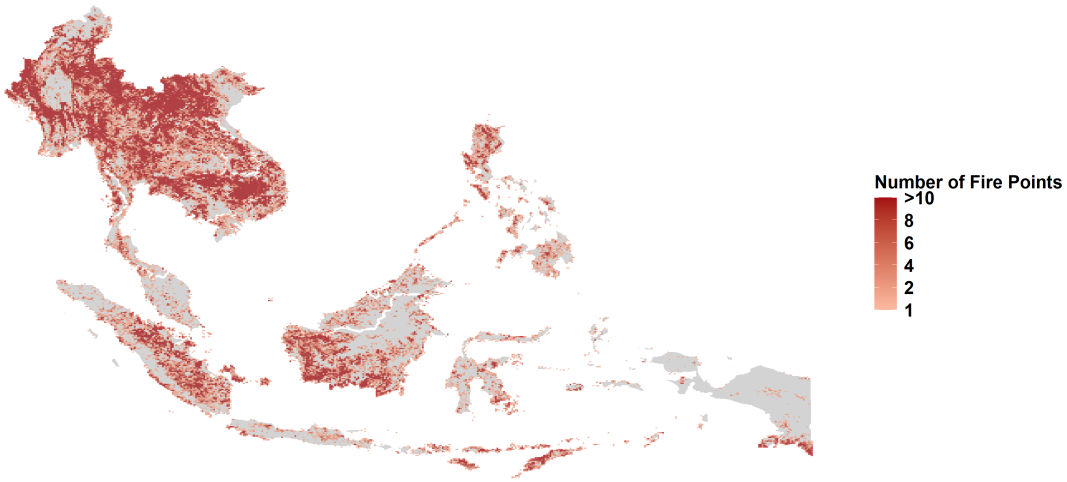

(A) Fire Activities Across Southeast Asia in 2003

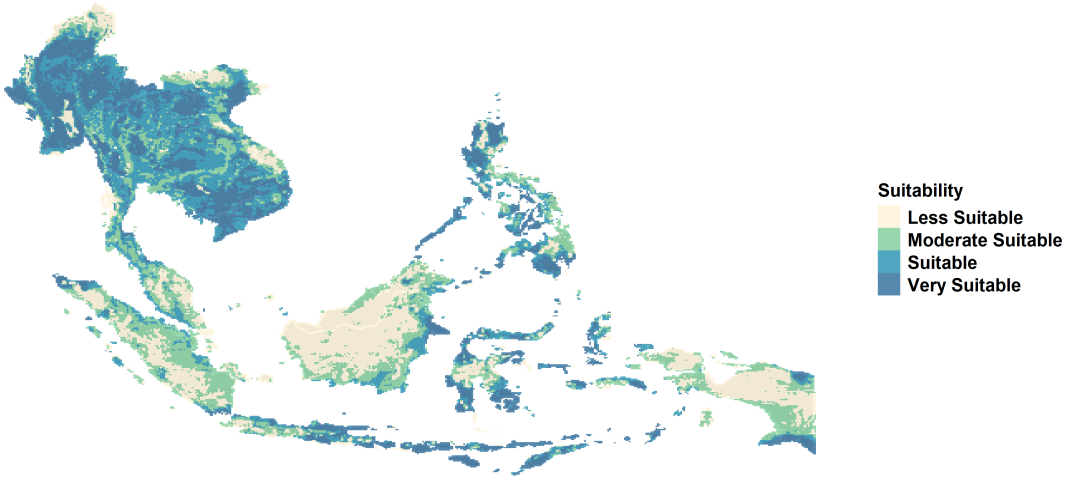

(B) Land Suitability Distribution in Southeast Asia

Figure 1: Distribution of Fire Activity and Suitability Across Lands in Southeast Asia

Notes: The figures show the distribution of fire activity and land suitability across Southeast Asia. Panel A displays the distribution of all fire points in 2003, while Panel B shows the distribution of land suitability across different levels. Suitability levels are calculated based on the potential yield values for all crops in Southeast Asia, with the potential yield data derived from the Global Agro-Ecological Zones (GAEZ) dataset.

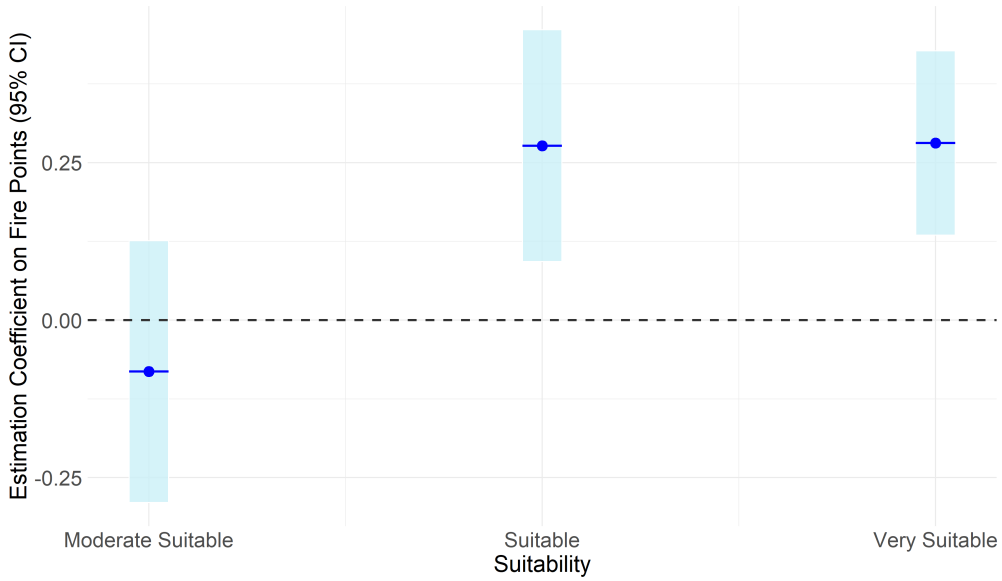

(A) Agricultural Export

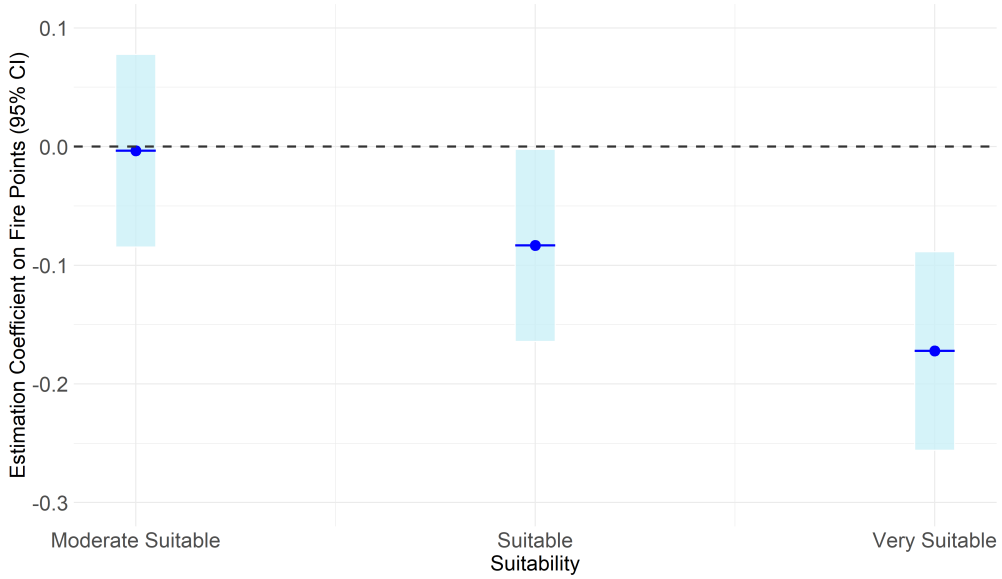

(B) MFN Tariff

Figure 2: The Impact of Trade on Fire Activity by Land Suitability

Notes: The figures illustrate the estimated impact of trade on fire activity across different levels of land suitability, based on Equation (7). The outcome variable is the number of fires in specific areas, and the mean value of the outcome variable is 4.63. Panel A shows the impact of agricultural exports, while Panel B illustrates the impact of MFN tariffs. *Moderate Suitable*, *Suitable*, and *Very Suitable* are dummy variables indicating the land suitability, which is derived from the Global Agro-Ecological Zones (GAEZ) dataset. The reference group consists of observations where the suitability falls in the "less suitable" or "not suitable" categories. All regressions include cell fixed effects and country-year fixed effects, as well as weather controls (precipitation, temperature, and PDSI, a dryness index). Other controls include cell-level characteristics interacted with year dummies, such as the number of fire points in each grid and whether the grid had cropland in the base year of 2003. Standard errors are clustered at the cell level.

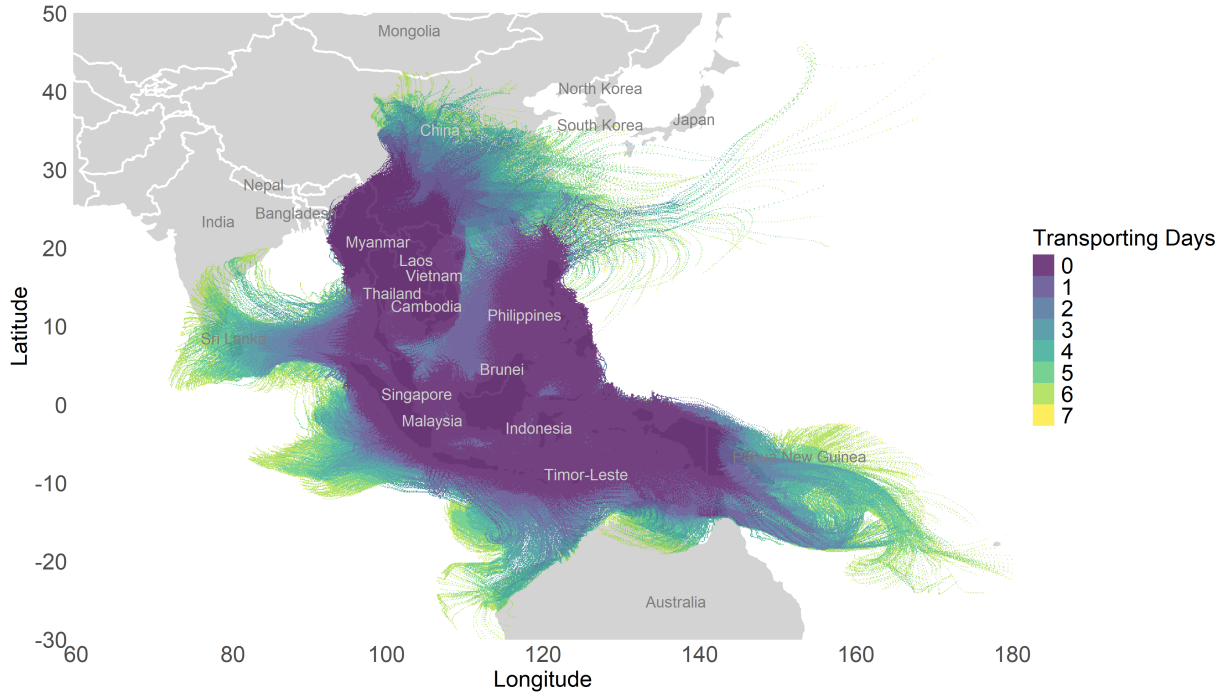

(A) Pollution Trajectories from Southeast Asia in March 2003

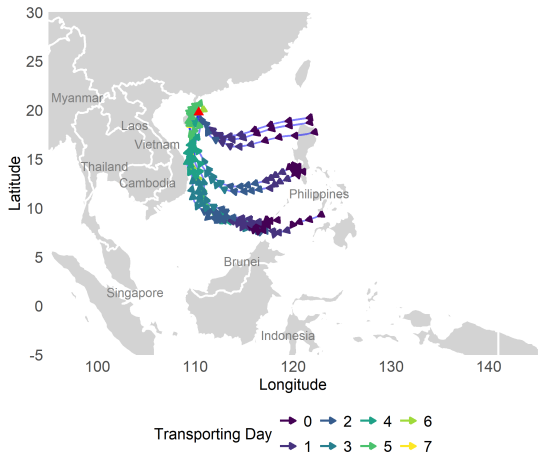

(B) Trajectories to Haikou, China

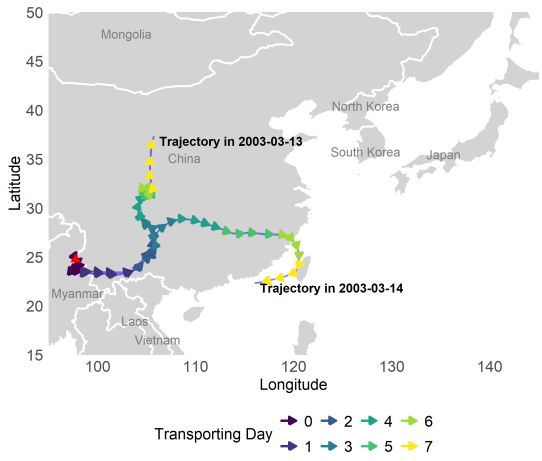

(C) Trajectories From Myanmar

Figure 3: Illustration of Pollution Transport Trajectories in Southeast Asia

Notes: The figures plot one-week pollution trajectories originating from Southeast Asia in March 2003. Panel A shows all pollution trajectories from Southeast Asia during that month. Panel B focuses on the trajectories from Southeast Asia to Haikou in March 2003. Panel C illustrates two specific one-week trajectories from Myitkyina, Myanmar (March 13, 2003, and March 14, 2003). All trajectories are simulations generated using the HYSPLIT model from NOAA.

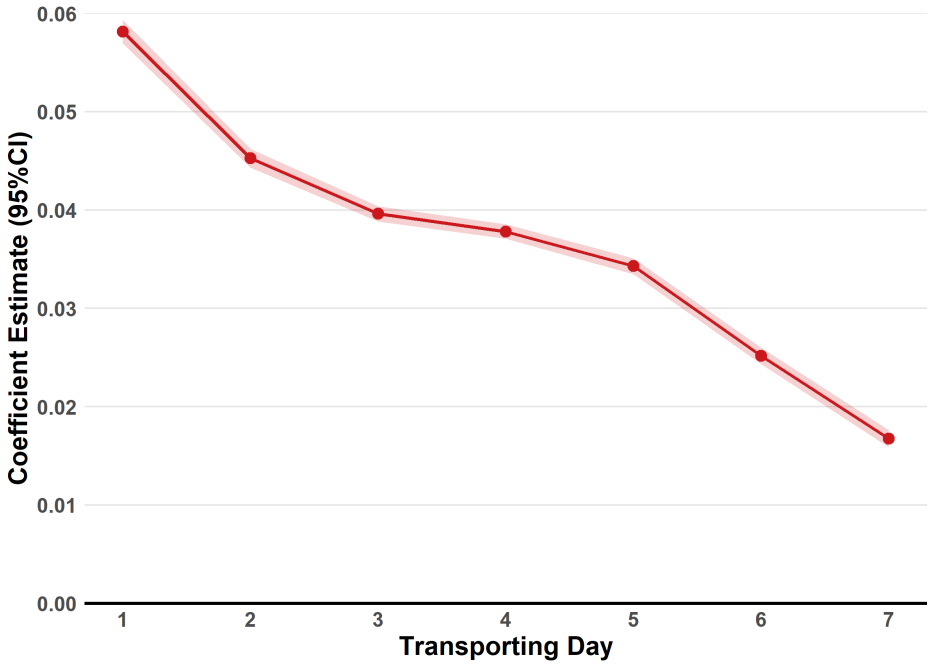

Figure 4: The Impact of Fires on Downstream Pollution Across Transporting day

Notes: The figure plots the estimated impact of one additional fire on downwind $PM_{2.5}$ by transporting day $w = 1, \ldots, 7$ (Equation (12)). Coefficients decline monotonically with w, with the largest effect on day 1 and much smaller effects by day 7.

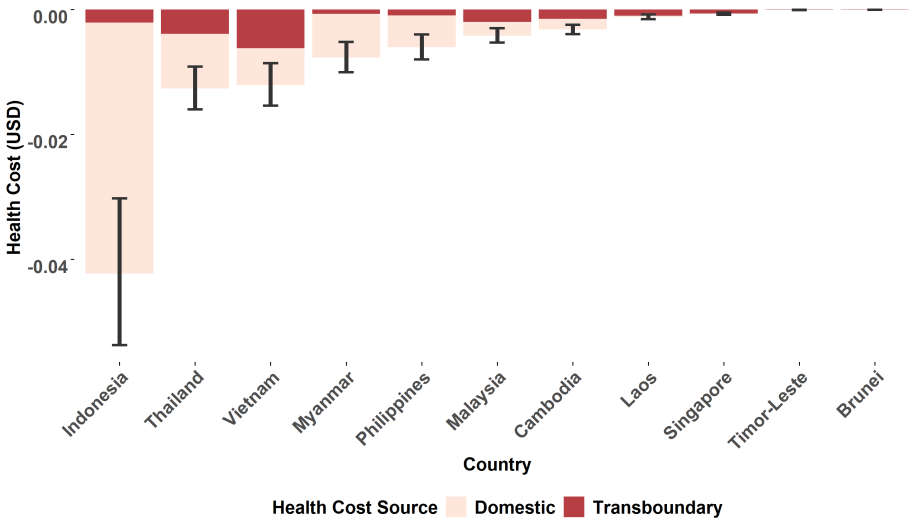

(A) Pollution Cost in Southeast Asia Countries

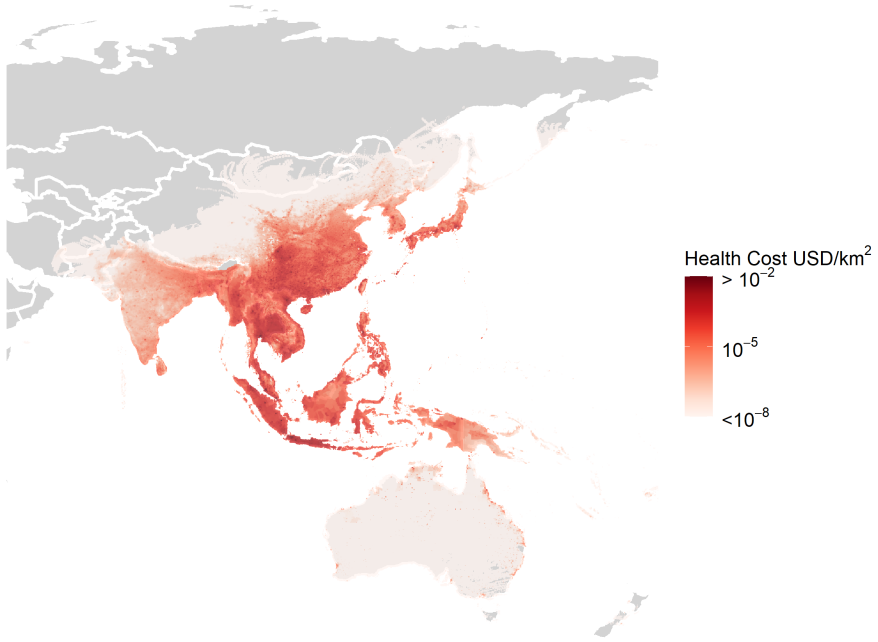

(B) Distribution of Pollution Cost

Figure 5: Costs of Trade-induced Fires from a 1 USD Increase in Agricultural Exports

Notes: The figures plot the pollution cost of trade-induced fires for each 1 USD increase in agricultural export value in the Southeast Asia (SEA) region. The pollution cost includes both morbidity and mortality costs, calculated according to Equation (14). Panel A displays the pollution costs in SEA countries resulting from a 1 USD increase in agricultural export value relative to the region's total export value, along with a 95% confidence interval (CI). The light red bars represent the costs from domestic fire smoke, while the dark red bars represent the costs from neighboring countries. Panel B shows the spatial distribution of pollution costs for the same 1 USD increase in agricultural export value. This map is based on a 0.1-degree grid and includes 2.7 $\times 10^5$ grids affected by fires from SEA. When agricultural export value increases by 1 USD, the total global cost is 0.115 USD.

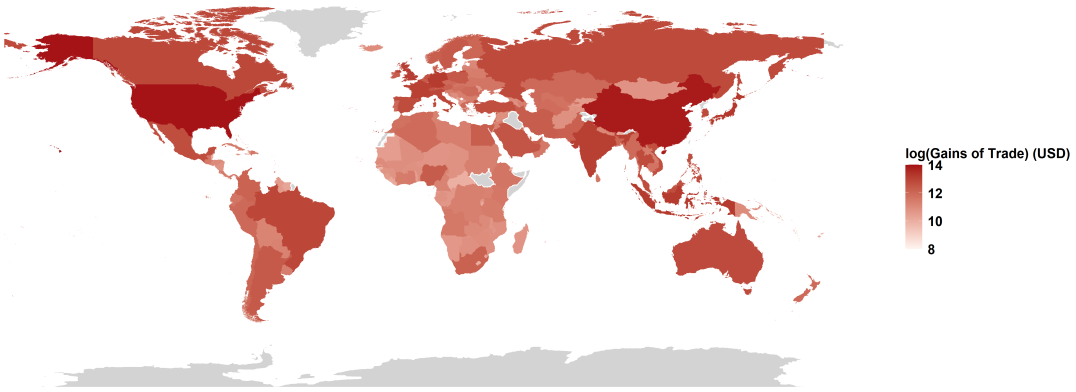

(A) Welfare Gains of Trading with SEA

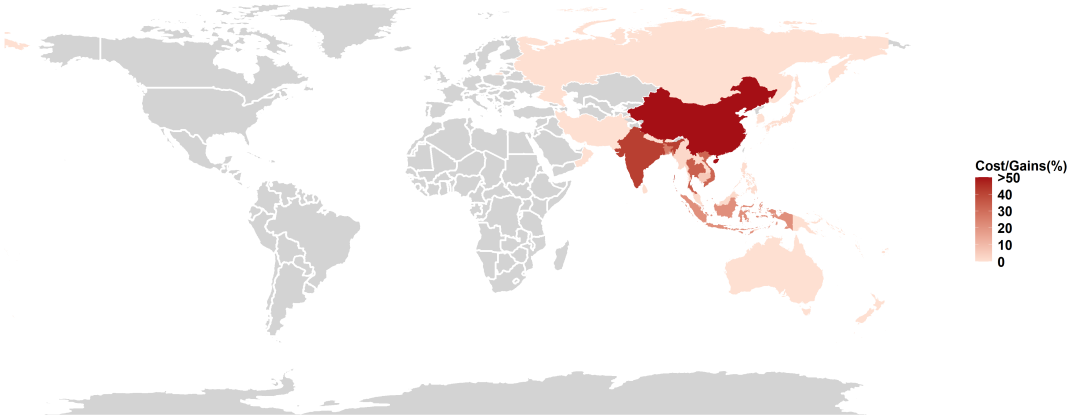

(B) Distribution of Pollution Costs Relative to Trade Gains

Figure 6: Benefits and Environmental Costs of Agricultural Trade with SEA

Notes: This figure shows the gains and costs of international agricultural trade with SEA countries. Gains and costs are obtained from a model comparing trade under 2021 conditions to a no-trade counterfactual scenario. Details can be found in Section 3. Panel A displays the log value of trade gains from international agricultural trade with SEA; all countries benefit from trade with SEA countries. Panel B shows the ratio of pollution costs to trade gains from SEA agricultural trade. Ratios range from 0% to 275%, with China experiencing the highest ratio. Grey regions represent countries without pollution exposure.

Table 1: Descriptive Statistics

Variables	N	Mean	Sd	Min	Max
	(1)	(2)	(3)	(4)	(5)
Panel A Fire Activities					
# fire	808830	4.753	10.979	0	646.000
# periodfire	808830	4.297	10.304	0	537.000
# noperiodfire	808830	0.455	2.665	0	383.000
Fire Radiative Power(FRP)	808830	14.941	30.447	0	2289.3
burnarea (km^2)	808830	11.145	24.756	0	971.012
CO_2 ($\times 10^7$ tons)	808830	110.323	295.604	0	15403.810
$PM_{2.5}$ ($\times 10^4$ tons)	808830	27.609	75.812	0	4080.072
Panel B Grid-level Characteristics					
Suit	808830	0.698	0.459	0	1.000
Potential Yield(kg/ha)	808830	2831.280	789.195	0	4808.378
Forest Coverage(%)	808830	44.703	39.744	0	100.000
Cropland Coverage(%)	808830	13.182	28.645	0	100.000
Precipitation(mm)	808830	2438.948	1011.114	376.833	9747.800
PDSI	808830	4.874	34.118	-235.136	276.958
Max Temperature (°)	808830	32.234	29.677	7.233	41.300
Min Temperature (°)	808830	18.423	52.203	-22.117	26.383
Panel C: Trade Measures and Country-level Socio-Economic Characteristics					
Agricultural Export($\times 10^9$ USD)	209	10.697	13.079	0.001	56.927
non-Agricultural Export($\times 10^9$ USD)	209	104.315	111.952	0.004	437.488
MFN Tariff	209	13.62687	0.626	12.905	15.212
GDP ($\times 10^9$ USD)	209	202.171	229.015	0.877	1065.709
Population ($\times 10^6$)	209	56.170	71.256	.347	276.758

Notes: Observations in Panels A and B are at the cell-year level, while Panel C describes observations at the country-year level, covering the period from 2003 to 2021. Each cell has a 0.1°×0.1°resolution. Panel A summarizes all variables related to fire activities. # fire represents the annual number of fires for each grid, while # periodfire and # noperiodfire indicate the number of fires during the land clearing and planting periods, respectively. Fire Radiative Power (FRP) measures the average intensity of thermal anomalies, defined as the rate of radiant heat output, which is associated with the rate of fuel consumption and smoke emissions. Burning Area refers to the total annual burning area for each grid. CO_2 and $PM_{2.5}$ represent the fire-released CO_2 and $PM_{2.5}$ emissions, measured in tons. In Panel B, Suit is a dummy variable that equals one for grids where at least one crop falls into the categories of moderate suitability, high suitability, or very high suitability. Potential Yield refers to the average yield across all crops, measured in kilograms per hectare (kg/ha), and is obtained from the GAEZ (Global Agro-Ecological Zones) dataset. Forest Coverage and Cropland Coverage represent the annual percentage of land covered by forests and croplands, respectively. The Weather Controls include variables for annual precipitation, minimum temperature, maximum temperature, and the Palmer Drought Severity Index (PDSI), which measures dryness. Panel C presents country-level statistics for key variables. Agricultural Export and Non-agricultural Export represent the export values in the agricultural and non-agricultural sectors, respectively, measured in billions of USD ($\times 10^9$ USD). MFN Tariff is the simple average of the MFN tariff rates across all importers of Southeast Asian countries. GDP (in billions of USD, $\times 10^9$ USD) and Population (in millions, $\times 10^6$) refer to the GDP and population of each Southeast Asian country, respectively.

Table 2: Impact of Agricultural Exports on Land Use and Fire Points in Southeast Asia

	(1)	(2)	(3)	(4)
VARIABLES	Forest Change	Cropland Change	#Fires Clearing Period	#Fires Planting Period
log(AgExport) × Suit	-0.1124***	0.0673***	0.4064***	0.0214
	(0.0159)	(0.0072)	(0.0544)	(0.0152)
Observations	808,830	808,830	808,830	808,830
R-squared	0.1403	0.1057	0.5659	0.2888
Cell FE	Yes	Yes	Yes	Yes
Country FE X Year FE	Yes	Yes	Yes	Yes
Weather Controls	Yes	Yes	Yes	Yes
Other Controls	Yes	Yes	Yes	Yes

Notes: This table shows the impact of agricultural exports on the number of fire points at the grid level using Equation (8). log(AgExport) is the log of agricultural export values. Suit includes grids where at least one crop falls into moderate suitability, high suitability, and very high suitability. Forest Change in Column (1) and Cropland Change in Column (2) both represent the annual percentage change in forest and cropland coverage, respectively. Column (3) refers to the number of fires during the agricultural land clearing period, while Column (4) refers to the number of fires during the agricultural planting period. The classification of these periods is determined by the specific planting and cultivation seasons of each country. All regressions include cell fixed effects and country-year fixed effects. Weather controls include precipitation, temperature, and PDSI (a dryness index). Other controls include cell-level characteristics times year dummy and cell-level characteristics are the number of fire points in each grid and whether the grid had cropland in the base year of 2003. Standard errors are clustered at the cell level. *Significance levels: ***$p < 0.01$, **$p < 0.05$, *$p < 0.10$.

Table 3: Impact of Agricultural Exports on Fire Activities and Fire-induced Emission in Southeast Asia

VARIABLES Unit	(1) Burning Area km^2	(2) CO_2 10^7 tons	(3) $PM_{2.5}$ 10^4 tons	(4) FRP megawatts (MW)
log(AgExport) × Suit	1.0236***	9.4181***	2.1489***	0.7413***
	(0.1367)	(1.5205)	(0.3899)	(0.1518)
Observations	808,830	808,830	808,830	808,830
R-squared	0.6122	0.5460	0.5416	0.4909
Cell-Country FE	Yes	Yes	Yes	Yes
Country FE X Year FE	Yes	Yes	Yes	Yes
Weather Controls	Yes	Yes	Yes	Yes
Other Controls	Yes	Yes	Yes	Yes

Notes: This table shows the impact of agricultural exports on the number of fire points at the grid level using Equation (8). log(AgExport) is the log of agricultural export values. Suit includes grids where at least one crop falls into moderate suitability, high suitability, and very high suitability. The outcome variable in Column (1) represents the yearly burning area in km^2, while Column (2) measures the yearly CO_2 emissions from fires in 10^7 tons. Column (3) quantifies the impact on the yearly fire-emitted $PM_{2.5}$ in 10^4 tons. Column (4) shows the impact on the yearly FRP in megawatts, representing the total heat emitted by fires as a measure of fire intensity. All regressions include cell fixed effects and country-year fixed effects. Weather controls include precipitation, temperature, and PDSI (a dryness index). Other controls include cell-level characteristics times year dummy. Cell-level characteristics are the number of fire points in each grid and whether the grid had cropland in the base year of 2003. Standard errors are clustered at the cell level. *Significance levels: $***p < 0.01$, $**p < 0.05$, $*p < 0.10$.

A Tables and Figures

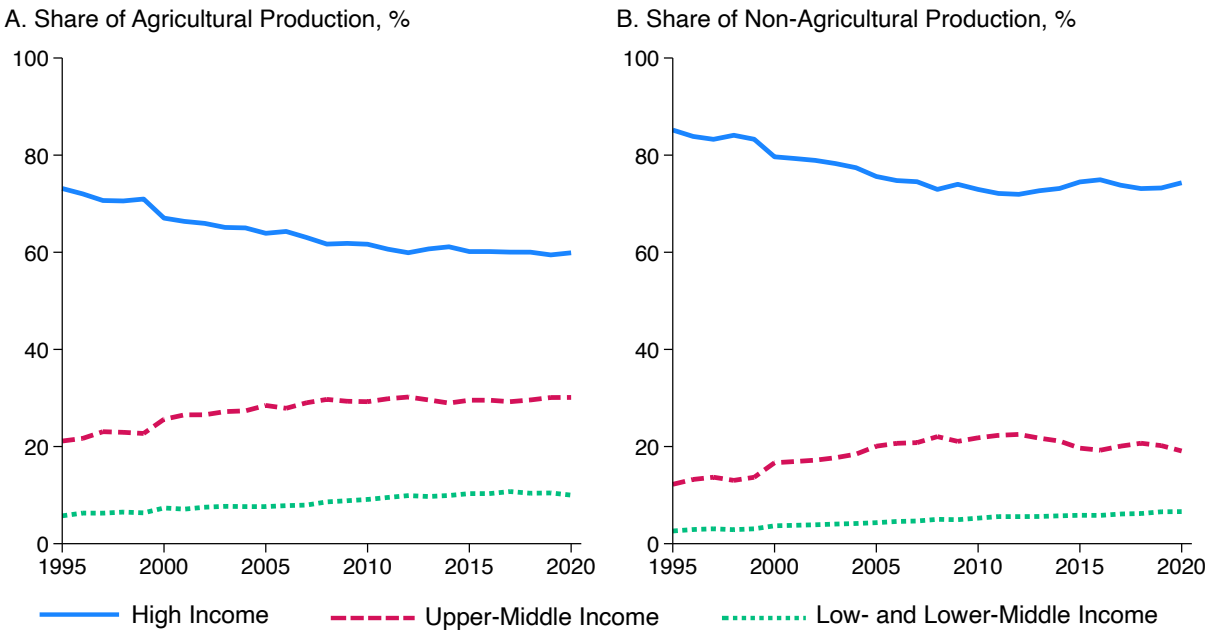

Figure A1: Production Share in Different Country Groups

Notes: The figure presents the share of agricutural and non-agricultural productions in different country groups. According to the World Bank's income classification for 2003, most Southeast Asian economies were categorized as low- or lower-middle-income countries. Singapore and Brunei were classified as high-income economies, Malaysia as an upper-middle-income economy, and Thailand as a lower-middle-income economy. Other countries in the region—including Indonesia, the Philippines, Vietnam, Cambodia, Laos, and Myanmar—belonged to the lower-middle- or low-income group. Data Source: World Bank.

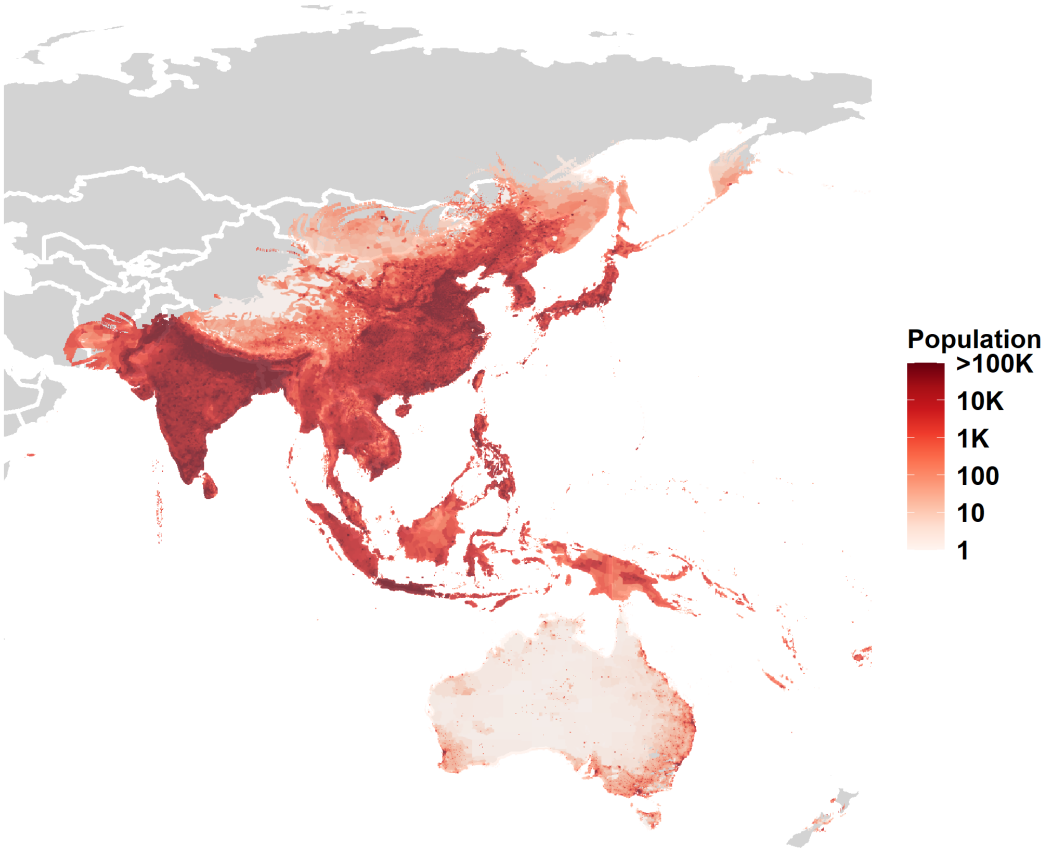

Figure A2: Population Exposure to Pollution From Southeast Asia

Notes: The figure shows the population distribution in regions potentially exposed to pollution from Southeast Asia. The unit for population is people per hectare. Exposure to pollution is defined as the areas impacted by the one-week pollution trajectories originating from Southeast Asia between 2003 and 2021. The grey region represents the non-affected area. In total, the affected areas impact approximately 4.2 billion people worldwide. Population data represent the grid-level population in 2020, obtained from the Gridded Population of the World, Version 4 (GPWv4).

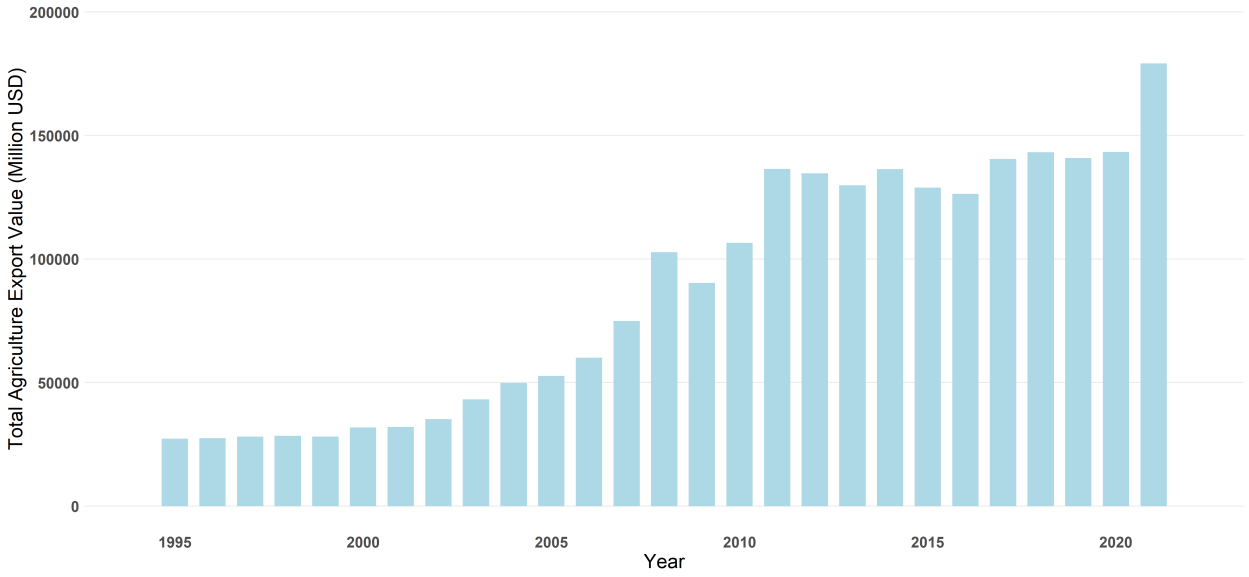

(A) Agricultural Export

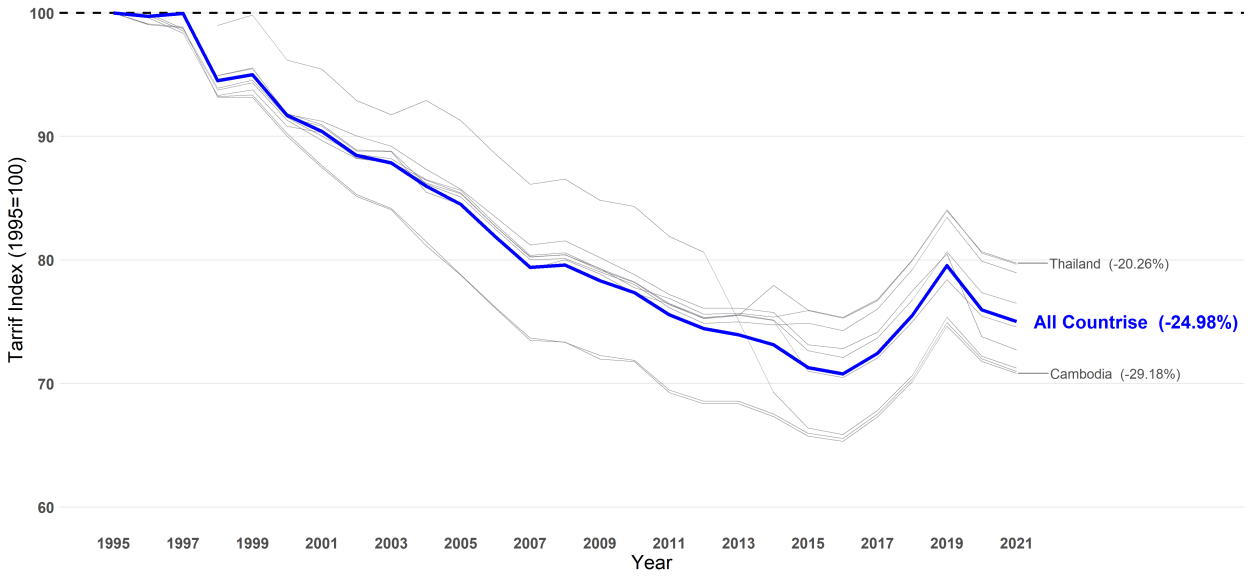

(B) Agricultural Export Tariff

Figure A3: Time Trend of Agricultural Export and Tariff in Southeast Asia

Notes: The figures show trends in agricultural export value and tariffs for Southeast Asia from 1995 to 2021. Panel A presents the region's total agricultural export value. Panel B shows the percentage change in the average agricultural export tariff relative to its 1995 level (1995 = 100), with individual country trends in grey and the regional average highlighted in blue. The analysis covers agricultural sectors corresponding to HS codes 01-24. The tariff measure is the simple average of preferential rates applied to trade between Southeast Asian nations and their partners.

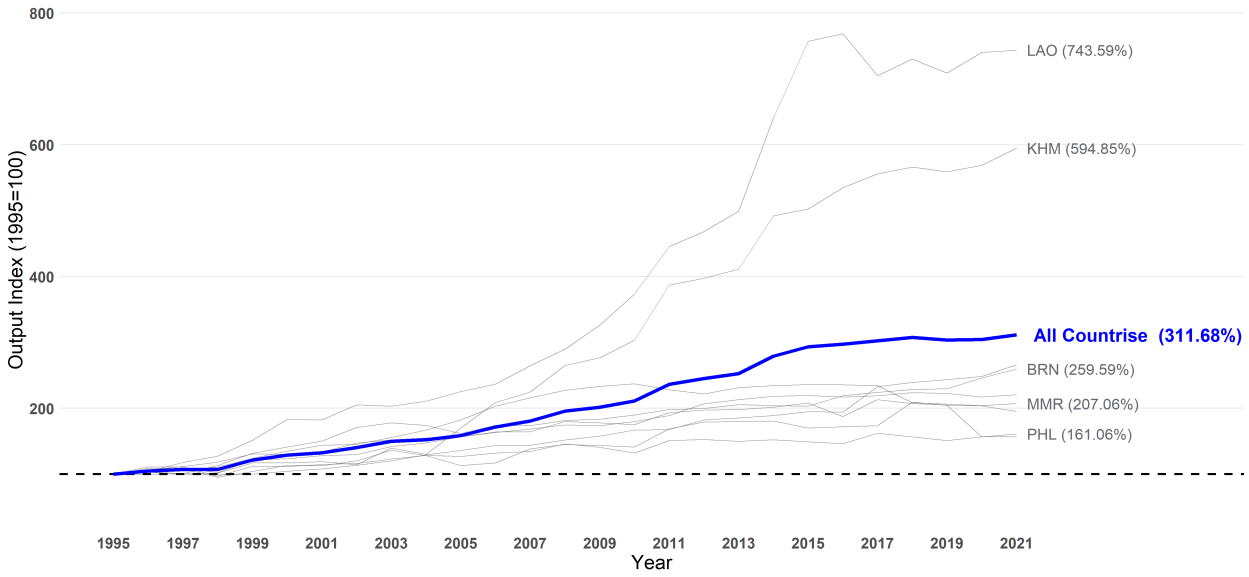

(A) Agricultural Output

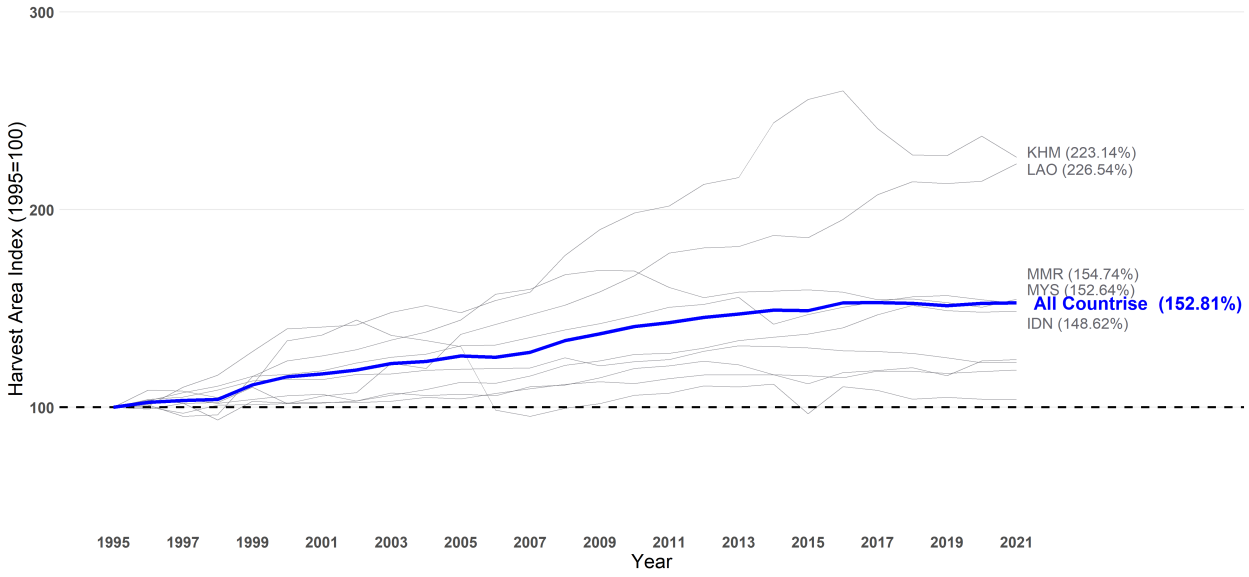

(B) Agricultural Harvest Area

Figure A4: Time Trend of Agricultural Output and Harvest Area in Southeast Asia

Notes: The figures show the time trend of agricultural output and harvested area in Southeast Asia from 1995 to 2021, expressed as percentage changes relative to the base year (1995=100). Grey lines represent individual countries, while the blue line refers to the regional average. Both "Output" and "Harvested Area" are measured as the total value and total area across all crop types.

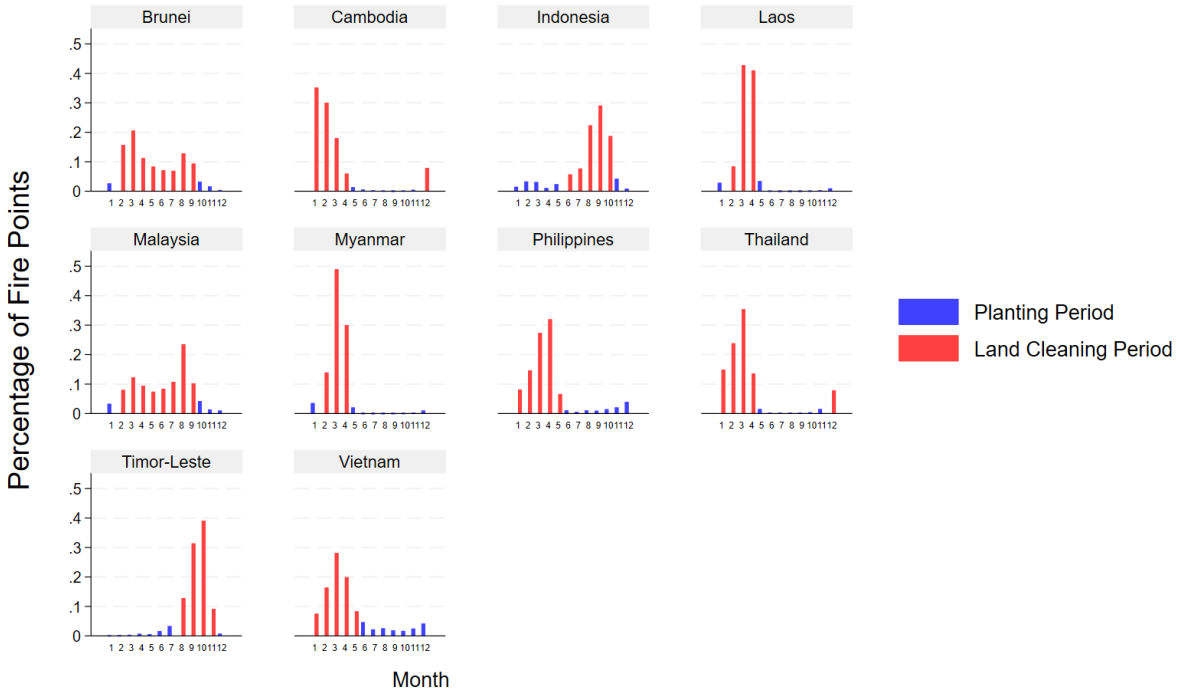

Figure A5: Fire Activities Across Months in Southeast Asia

Notes: The figure shows fire activity across months by country in Southeast Asia. The red bars represent the land-clearing period, while the blue bars indicate the planting period. Months in which fire activity exceeds 5% of the annual total are classified as the land-clearing period; otherwise, they are categorized as the planting period.

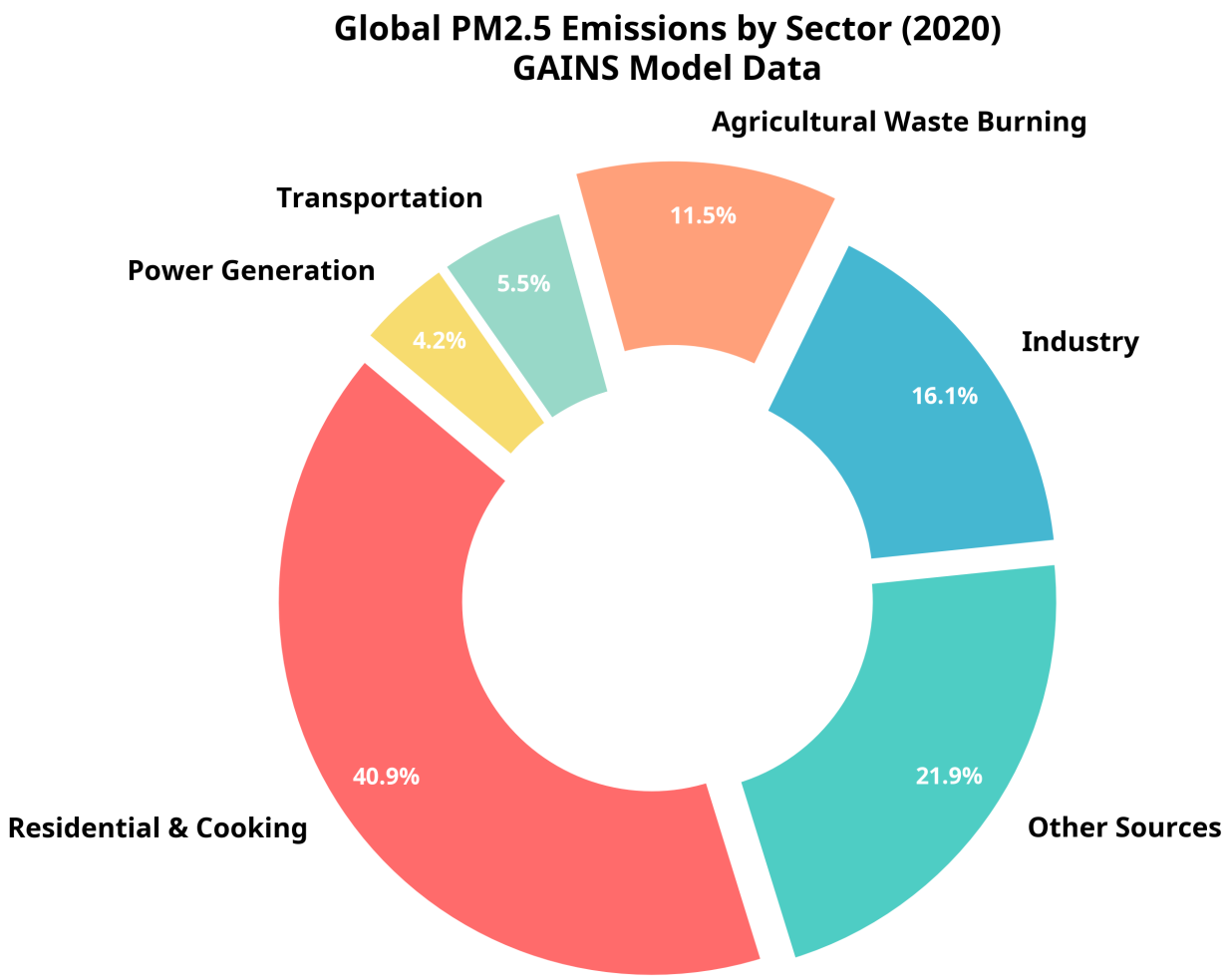

Figure A6: Global $PM_{2.5}$ Emissions by Source (2020)

Notes: This figure shows the distribution of global $PM_{2.5}$ emissions by economic sector based on Greenhouse Gas and Air Pollution Interactions and Synergies (GAINS) data for 2020. Agricultural Waste Burning accounts for 11.5% of global emissions, making it the third-largest single category.

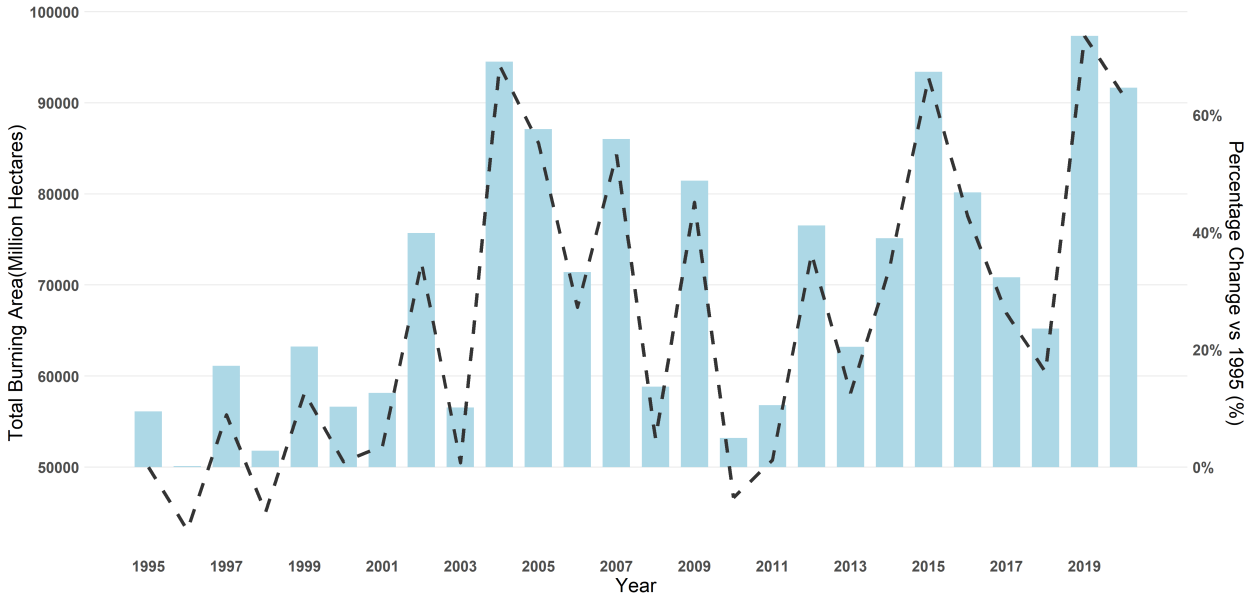

Figure A7: Time Trend of Changes in Total Burning Area in Southeast Asia

Notes: The figure depicts the time trend of changes in the total burned area across Southeast Asia from 1995 to 2021. The blue bars represent the annual total burned area (in hectares), while the dashed line shows the percentage change relative to the 1995 level.

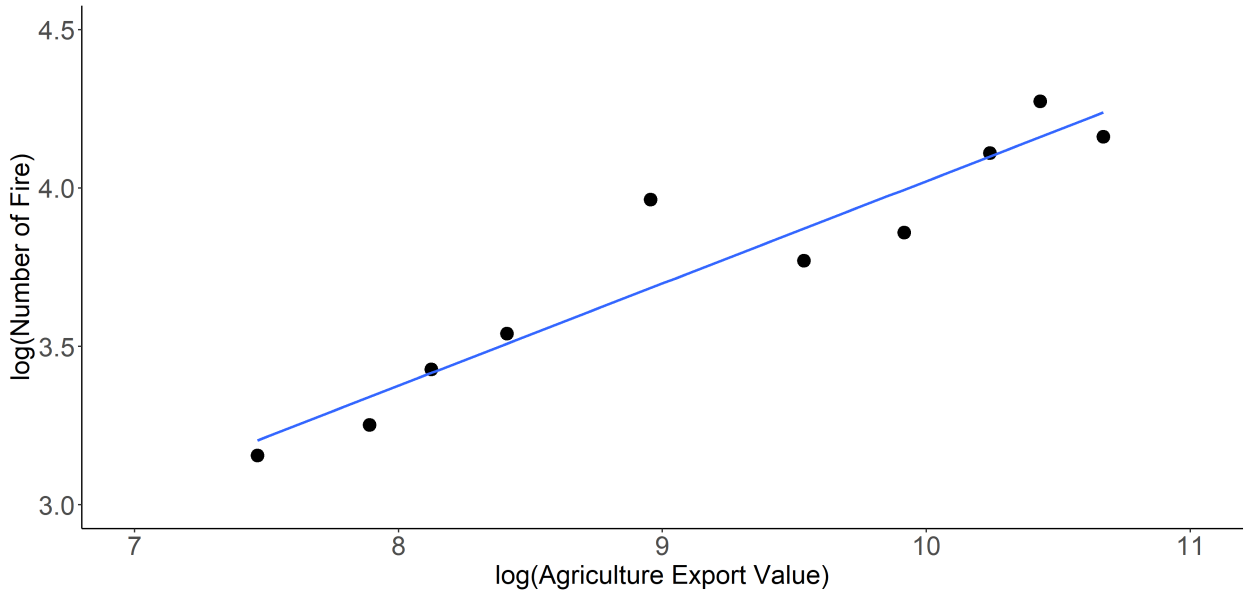

Figure A8: Binscatter Plot of Agricultural Exports and Fire Activity

Notes: The figure presents a binscatter plot showing the relationship between the log of agricultural exports and the log of the number of fires at the country-year level. The data is grouped into 10 bins. The bin regression includes weather controls such as precipitation, temperature, and the Palmer Drought Severity Index (PDSI).

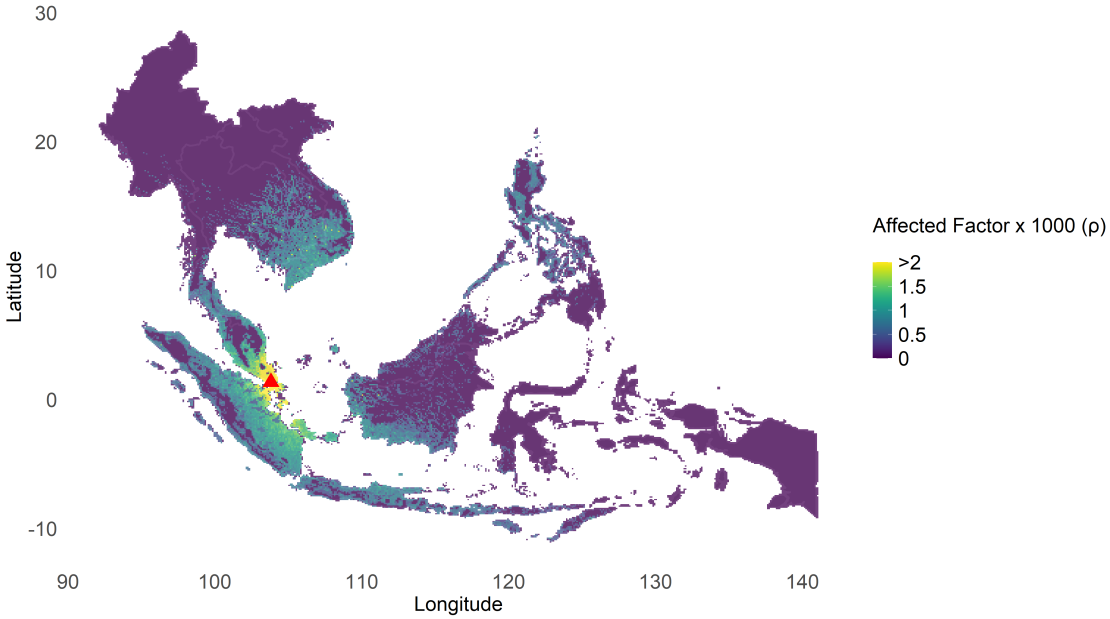

Figure A9: The Impact of Fires on Pollution in Singapore

Notes: The figures illustrate how fires in other SEA grid cells influence air pollution in Singapore, representing the spatial effect ρ_{ij} with j = Singapore. Here, the impact factor ρ_{ij} is computed using Equation (13). The red point represents the location of Singapore.

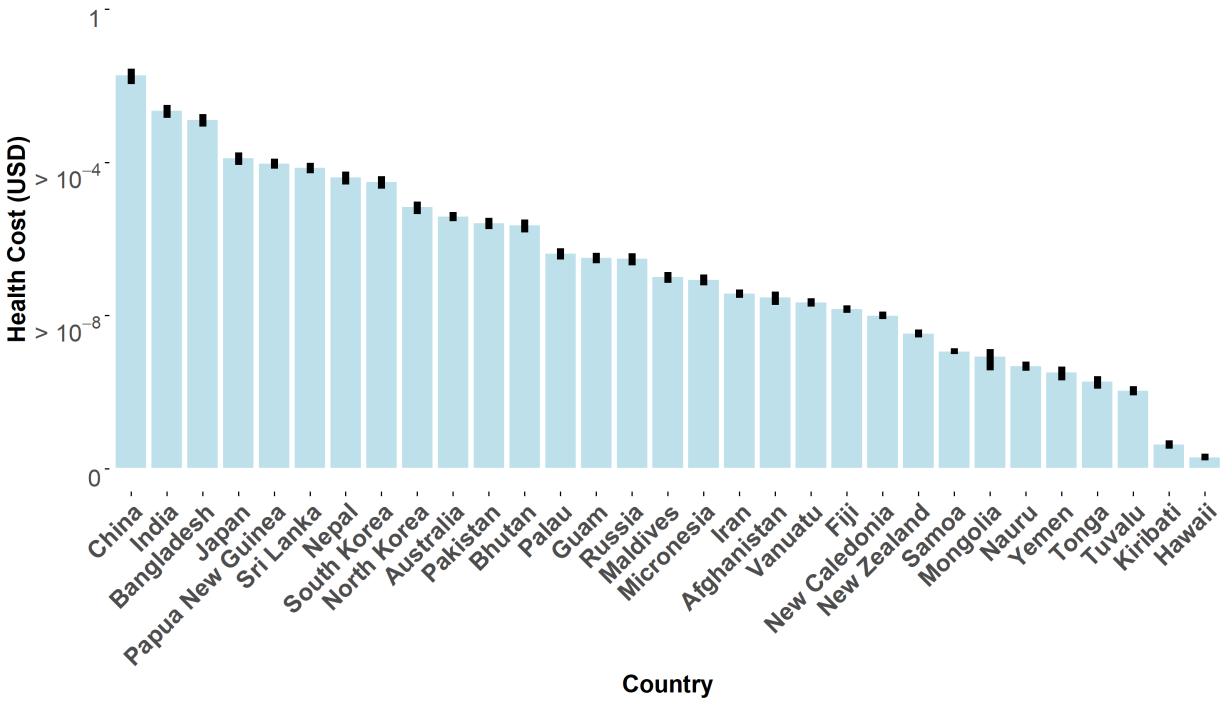

Figure A10: Costs of Trade-induced Fires from a 1 AgExport USD Increase

Notes: The figures illustrate the pollution cost of trade-induced fires in non-SEA countries for each 1 USD increase in agricultural export value from the Southeast Asia (SEA) region. The pollution cost includes both morbidity and mortality costs, calculated according to Equation (14). When the agricultural export value from SEA increases by 1 USD, the total pollution cost in non-SEA regions is 0.024 USD.

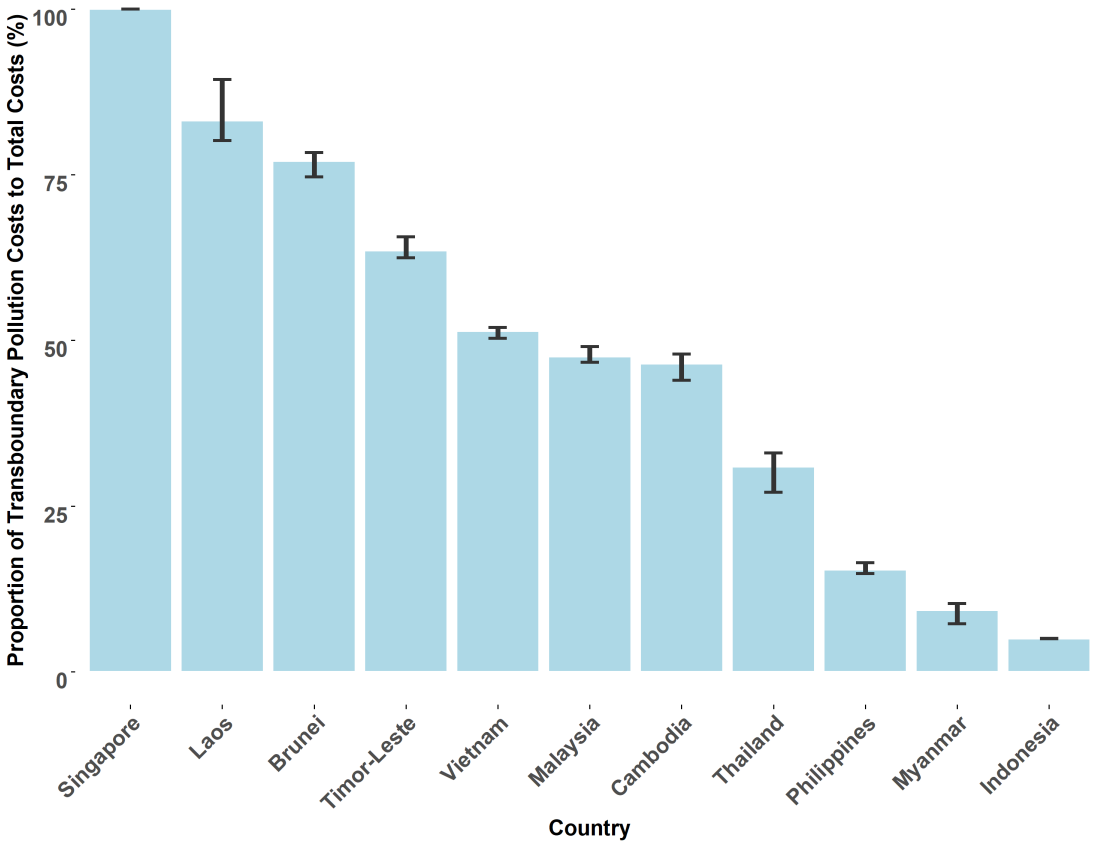

Figure A11: Proportion of Transboundary Pollution Costs to Total Costs in Southeast Asia

Notes: The figure depicts the proportion of transboundary pollution costs relative to total costs in Southeast Asia. Pollution costs are calculated using Equation (14), with transboundary pollution referring to pollution originating from other countries.

Table A1: Extensive and Intensive Margin: Impact of Trade on Fire Activities

	(1) Have Fire	(2) log(# Fires)	(3) Have Fire	(4) # Fires
log(AgExport) × Suit	0.0007	0.0542***	0.0070*	0.0850***
	(0.0019)	(0.0075)	(0.0036)	(0.0095)
Marginal Effect			0.00434*	0.516***
		(0.00227)		(0.0579)
Observations	808,830	391,911	632,567	632,567
R-squared	0.6295	0.6304		
Cell-Country FE	Yes	Yes	Yes	Yes
Country FE X Year FE	Yes	Yes	Yes	Yes
Weather Controls	Yes	Yes	Yes	Yes
Other Controls	Yes	Yes	Yes	Yes
Model	OLS	OLS	PPML	PPML

Notes: This table shows the extensive and intensive margins impact of agricultural exports on the number of fire points at the grid level using the Equation (8). log(AgExport) is the log of agricultural export values. Suit includes grids where at least one crop falls into moderate suitability, high suitability, and very high suitability. Have Fire is a dummy variable equal to one if the grid has fire points in a given year. # Fires represents the number of fire points in a specific year. Columns (1) and (2) measure the extensive and intensive margins of the impact on fire activity using OLS regression, respectively, while Columns (3) and (4) use the PPML regression model. All regressions include cell fixed effects and country-year fixed effects. Weather controls include precipitation, temperature, and PDSI (a dryness index). Other controls include cell-level characteristics times year dummy. Cell-level characteristics are the number of fire points in each grid and whether the grid had cropland in the base year of 2003. Standard errors are clustered at the cell level. *Significance levels: ***$p < 0.01$, **$p < 0.05$, *$p < 0.10$.

Table A2: Robustness Check: Estimation using Potential Yield Suitability

VARIABLES	(1) # Fires	(2) Burning Area km^2	(3) CO_2	(4) $PM_{2.5}$
Unit			10^4 tons	10^4 tons
log(AgExport) × Potential Yield	0.0008***	0.0016***	11.0789***	7.8709***
	(0.0000)	(0.0001)	(0.6340)	(0.5969)
Observations	808,830	808,830	808,830	808,830
R-squared	0.5490	0.5988	0.5312	0.5259
Cell FE	Yes	Yes	Yes	Yes
Country FE X Year FE	Yes	Yes	Yes	Yes
Weather Controls	Yes	Yes	Yes	Yes
Other Controls	Yes	Yes	Yes	Yes

Notes: This table shows the impact of agricultural exports on the number of fire points at the grid level using the Equation (8). log(AgExport) is the log of agricultural export values. Potential Yield refers to the average potential yield of all crops that can be planted in the grids, with the unit expressed in kilograms per hectare (kg/ha). # Fires in Column (1) and (2) represent the number of fire points in a specific year. Column (3) measures the yearly CO_2 emissions from fires in 10^4 tons. Column (4) quantifies the impact on the yearly fire-emitted $PM_{2.5}$ in 10^4 tons. All regressions include cell fixed effects and country-year fixed effects. Weather controls include precipitation, temperature, and PDSI (a dryness index). Other controls include cell-level characteristics times year dummy. Cell-level characteristics are the number of fire points in each grid and whether the grid had cropland in the base year of 2003. Standard errors are clustered at the cell level. *Significance levels: $^{***}p < 0.01$, $^{**}p < 0.05$, $^{*}p < 0.10$.

B Robustness Check: Crop-Specific Export Shocks

In Section 5, we aggregate suitability across crops and use total agricultural export values for each country to capture the broader impacts of agricultural trade shocks. In this appendix, we adopt a crop-specific approach to examine the robustness of our findings.

B1 Construction of Exposure Measures

We construct two measures of trade exposure that exploit variation in crop-specific export shocks and local agricultural suitability, differing in how they weight the importance of each crop-grid combination.

ExportPenetration captures within-grid variation in crop composition. The intuition is straightforward: a grid is more exposed to shocks in crops for which it has higher agro-ecological suitability compared to other crops in that same grid. Specifically, we define:

$$ExportPenetration_{cit} = \sum_{g} \frac{PotentialYield_{cig}}{\sum_{g} PotentialYield_{cig}} \times \log(Export_{cgt}) \tag{B.1}$$

where $PotentialYield_{cig}$ represents the potential yield of crop g in grid i, country c, and $Export_{cgt}$ denotes the export value of crop g from country c in year t. The weights $\frac{PotentialYield_{cig}}{\sum_{g} PotentialYield_{cig}}$ capture the relative suitability of each crop within the grid. Grids with no suitability for any crop receive zero weight and are thus assumed to be unaffected by export shocks.

ExportExposure captures within-country variation in the spatial distribution of crop production potential. The logic here is that grids that are relatively more suitable for a particular crop compared to other grids in the country should experience larger responses to shocks in that crop's exports—such grids are more likely to be converted to agricultural use when export demand rises. The definition is as follow:

$$ExportExposure_{cit} = \sum_{g} \frac{PotentialYield_{cig}}{\sum_i PotentialYield_{cig}} \times \log(Export_{cgt}) \tag{B.2}$$

The weights $\frac{PotentialYield_{cig}}{\sum_i PotentialYield_{cig}}$ capture each grid's importance in the country's total production potential for crop g. This measure reflects the intuition that when exports of crop g increase, agricultural expansion and fire activity should intensify more in grids that account for a larger share of the country's suitability for that crop.

B2 Instrumental Variable Strategy

To address potential endogeneity concerns, we employ a shift-share instrumental variable design. Our instrument exploits variation in importers' MFN tariff rates, which are plausibly exogenous to local fire activity in exporting countries. For ExportPenetration:

$$ExportPenetrationMFN_{cit} = \sum_{g} \frac{PotentialYield_{cig}}{\sum_g PotentialYield_{cig}} \times MFN_{cgt} \tag{B.3}$$

And for ExportExposure:

$$ExportExposureMFN_{cit} = \sum_{g} \frac{PotentialYield_{cig}}{\sum_i PotentialYield_{cig}} \times MFN_{cgt} \tag{B.4}$$

where MFN_{cgt} represents the MFN tariff rate faced by crop g from country c in year t. The identifying assumption is that changes in importers' tariff policies are determined by importing countries and are unlikely to be correlated with local environmental conditions in exporting regions.

B3 Empirical Specification

We estimate both reduced-form and two-stage least squares (2SLS) specifications.

Reduced Form. We first estimate the direct effect of the tariff-based instrument on fire

activity:

$$Fire_{cit} = \alpha + \lambda ExportExposureMFN_{cit} + \gamma' \mathbf{X}it + \theta ct + \tau_t + \pi_i + \varepsilon_{cit} \tag{B.5}$$

where $ExportExposureMFN_{cit}$ is the shift-share instrument defined in Equation B.4 (or $ExportPenetrationMFN_{cit}$ from Equation B.3 in alternative specifications). The coefficient λ captures the reduced-form effect of tariff-induced trade shocks on fire activity.

Two-Stage Least Squares. Our 2SLS specification proceeds as follows. The first stage estimates the effect of the instrument on trade exposure:

$$ExportExposure_{cit} = \alpha + \delta ExportExposureMFN_{cit} + \gamma' \mathbf{X}it + \theta ct + \tau_t + \pi_i + \varepsilon_{cit} \tag{B.6}$$

The second stage examines the impact of instrumented trade exposure on fire activity:

$$Fire_{cit} = \alpha + \beta \widehat{ExportExposurecit} + \gamma' \mathbf{X}it + \theta_{ct} + \tau_t + \pi_i + \varepsilon_{cit} \tag{B.7}$$

In these specifications, $ExportExposure_{cit}$ refers to either the ExportExposure measure (Equation B.2) or the ExportPenetration measure (Equation B.1), with corresponding instruments. $Fire_{cit}$ represents fire activity in grid i, country c, and year t. Our primary outcome is the number of fire points, though we also examine burned areas and pollutant emissions as alternative outcomes in robustness checks.

The key explanatory variable in the second stage measures a grid's exposure to crop-specific export shocks weighted by its relative production potential. The coefficient β reveals the causal impact of trade-induced agricultural expansion on local fire activity, capturing the direct effects in areas suitable for export crops. Note that $\beta = \lambda/\delta$, relating the reduced-form and 2SLS estimates.

$\mathbf{X}it$ includes the control variables defined in Section 5. We include grid fixed effects (π_i), year fixed effects (τ_t), and country-year fixed effects (θct). The country-year fixed effects

are crucial as they allow us to compare grids with different exposure levels within the same country and year, absorbing country-level shocks to agricultural exports.

B4 Result

Crop-Specific Export Shocks. Table B1 examines the robustness of our findings using alternative measures of trade exposure that weight crop-specific export shocks by local agricultural suitability. This approach allows us to capture heterogeneous exposure across grids based on their comparative advantage in different crops.

Columns (1) and (2) present reduced-form estimates, directly relating MFN tariff-weighted instruments to fire activity. Both specifications show negative and statistically significant coefficients on the tariff instruments. To interpret the magnitudes, we evaluate the effects of a one-standard-deviation decrease in tariffs (reflecting trade liberalization). A one-standard-deviation reduction in ExportPenetrationMFN (3.75 percentage points) increases fire points by 1.31 ($= 0.348 \times 3.75$). A one-standard-deviation reduction in ExportExposureMFN (0.105 percentage points) increases fire points by 2.94 ($= 27.977 \times 0.105$). These results indicate that trade liberalization—manifested through lower tariffs faced by exporting countries—directly increases fire activity, consistent with the mechanism that tariff reductions stimulate agricultural exports and subsequent land-use change.

Columns (3) and (4) report the two-stage least squares estimates, where we instrument actual export exposure with the MFN tariff-based measures. The results confirm our main findings: increased agricultural export exposure significantly raises fire activity. To interpret the magnitudes, we evaluate the effects of a one-standard-deviation increase in each exposure measure. A one-standard-deviation increase in ExportPenetration (5.09 units) increases fire points by 3.20 ($= 0.629 \times 5.09$), representing approximately a 3.2% increase relative to the sample mean of 1 fire points per grid-year. Similarly, a one-standard-deviation increase in ExportExposure (0.065 units) increases fire points by 2.21 ($= 33.967 \times 0.065$), or roughly a 2.2% increase. Both measures thus yield economically similar and substantial effects. The

first-stage F-statistics exceed 6,990, indicating strong instruments.

These results demonstrate that our main findings are robust to alternative constructions of trade exposure that explicitly account for crop-level heterogeneity in both export shocks and local production potential. The fact that both weighting schemes—emphasizing within-grid crop composition and within-country spatial distribution—yield consistent positive effects strengthens confidence in the causal link between agricultural trade and fire activity.

Table B1: Robustness: Impact of Agriculture Export on Fire Activities (Crop-specific Agricultural Export)

	(1)	(2)	(3)	(4)
VARIABLES	#Fires	#Fires	#Fires	#Fires
	Reduced-form		IV	
ExportPenetrationMFN	-0.3481***			
	(0.0325)			
ExportExposureMFN		-27.9769***		
		(6.8643)		
ExportPenetration			0.6290***	
			(0.0564)	
ExportExposure				33.9674**
				(14.8522)
Mean-Independent Variable	13.625	0.039	17.640	0.039
Std-Independent Variable	3.750	0.105	5.090	0.065
Observations	808,830	808,830	808,830	808,830
R-squared	0.5617	0.5617	0.0031	0.0031
F-stat			6990.27	6990.27
Cell FE	Yes	Yes	Yes	Yes
Country FE X Year FE	Yes	Yes	Yes	Yes
Weather Controls	Yes	Yes	Yes	Yes
Other Controls	Yes	Yes	Yes	Yes

Notes: This table presents the impact of crop-specific agricultural export shocks on fire activity at the grid level. Columns (1) and (2) report reduced-form estimates using MFN tariff-based instruments weighted by different suitability shares (Equation B.5). Columns (3) and (4) report two-stage least squares estimates with instrumented trade exposure (Equation B.7). ExportPenetration measures trade exposure using within-grid crop yield shares as weights (Equation B.1). ExportExposure measures trade exposure using within-country grid yield shares for each crop as weights (Equation B.2). The dependent variable, Fires, is the number of fire points in a grid-year. All regressions include grid fixed effects and country-year fixed effects. Weather controls include precipitation, temperature, and PDSI (Palmer Drought Severity Index). Additional controls include baseline grid characteristics (number of fire points and cropland presence in 2003) interacted with year dummies. Standard errors are clustered at the grid level. $^{*}p < 0.10$, $^{**}p < 0.05$, $^{***}p < 0.01$.